Adv Polym Sci (2007) 209: 1–58
DOI 10.1007/12_2007_112

Published online: 24 March 2007

Functional Hyperbranched Macromolecules Constructed from Acetylenic Triple-Bond Building Blocks

Matthias Häußler · Ben Zhong Tang (✉)

Department of Chemistry, The Hong Kong University of Science & Technology, Clear Water Bay, Kowloon, Hong Kong,
and Department of Polymer Science and Engineering, Zhejiang University, 310027 Hangzhou, China
tangbenz@ust.hk

Abstract This review article summarizes the synthetic efforts in constructing functional hyperbranched macromolecules from acetylenic triple-bond building blocks. Polymerization reactions including polycoupling, polyaddition and polycyclotrimerization have been developed for the synthesis of new hyperbranched polymers such as polyynes, polyenes, polyarylenes and polytriazoles with novel topological structures and electronic conjugations. Polymers with high molecular weights (up to $> 1 \times 10^6$) have been obtained in high yields (up to 100%). Whilst their linear counterparts are often intractable, the hyperbranched conjugated polymers are completely soluble in common organic solvents and are hence readily processable by macroscopic techniques. The hyperbranched polymers exhibit an array of functional properties including strong light emission, stable optical

nonlinearity and high photorefractivity. The polymers can generate fluorescent images, assemble into supramolecular patterns, and form well-aligned nanotubes. The polyynes can be post-functionalized through metal complexation, whose refractive indexes can be manipulated to a great extent by photoirradiation. The hyperbranched polymer complexes can serve as precursors to soft ferromagnetic ceramics and as catalysts for carbon nanotube fabrications.

Keywords Functional materials · Hyperbranched polymers · Polyaddition · Polycoupling · Polycyclotrimerization

Abbreviations

AAO	anodic aluminum oxide
AFM	atomic force microscopy
Ar	aromatic ring
β	molecular first hyperpolarizability
Bu	butyl group
c	concentration
C	core molecule
CNT	carbon nanotube
Cp*	pentamethylcyclopentadienyl ligand
CVD	chemical vapor deposition
D	dendritic unit
$D_{0.5}$	dose needed for an F_g value of 0.5 (or 50%)
d_{33}	macroscopic SHG coefficient
DB	degree of branching
DCM	dichloromethane
D_e	exposure dose
DMF	*N*,*N*-dimethylformamide
DSC	differential scanning calorimetry
EO	electro-optical
F_g	gel fraction
F_{OL}	optical limiting threshold fluence
FTIR	Fourier-transfer infrared spectroscopy
$F_{t,m}/F_{i,m}$	optical signal suppression ratio
GPC	gel permeation chromatography
H	strength of magnetic field
hb-PA	hyperbranched polyarylene
hb-PAA	hyperbranched poly(aroylarylene)
hb-PAE	hyperbranched poly(aryleneethynylene)
hb-PAP	hyperbranched poly(alkylenephenylene)
hb-PP	hyperbranched polyphenylene
hb-PPE	hyperbranched poly(phenyleneethynylene)
hb-PTA	hyperbranched polytriazole
hb-PY	hyperbranched polyyne
H_c	coercivity
L	ligand
L	linear unit
l_f	film thickness
λ_{ab}	absorption maximum

λ_{em}	emission maximum
λ_{ex}	excitation wavelength
M	magnetization
M	monomer
Me	methyl group
M_n	number-average molecular weight
M_s	saturation magnetization
M_w	weight-average molecular weight
MWD	molecular weight distribution
NLO	Nonlinear optical
NMR	nuclear magnetic resonance spectroscopy
P	polymer
PB	polymer branch
PC	polycarbonate
PDI	polydispersity index (M_w/M_n)
PEO_{600}	poly(ethylene oxide) with a molecular weight of 600
pH	solution acidity
PH	poly(1-hexyne)
Φ_F	fluorescence quantum yield
pK_a	acidity constant
PL	photoluminescence
PMMA	poly(methyl methacrylate)
PPA	poly(phenylacetylene)
PPP	poly(*p*-phenylene)
PS	polystyrene
RI	refractive index (n)
S	solid support
SEC	size-exclusion chromatography
SEM	scanning electron microscope
SHG	second-harmonic generation
t	exposure time
T	terminal unit
T	terminator
T_d	thermal degradation temperature
TEM	transmission electron microscope
T_g	glass transition temperature
TGA	thermogravimetric analysis
THF	tetrahydrofuran
T_L	linear transmittance
TMEDA	N,N,N',N'-tetramethylethylenediamine
TPA	triphenylamine
UV	ultraviolet
W_r	weight residue after pyrolysis
X	halogen
XPS	X-ray photoelectron spectroscopy
XRD	X-ray diffraction

1 Introduction

Hyperbranched polymers have emerged as a new class of macromolecules that show architectural beauty and multifaceted functionality of dendrimers while enjoying the ease of being prepared by simple, single-step reaction procedures. A number of strategies have been developed for the synthesis of hyperbranched polymers. The commonly adopted approach is self-condensation polymerization of AB_x-type monomers with $x \geq 2$ where A and B are mutually reactive functional groups, dating back to the theoretical work of Flory in the early 1950s [1]. Because of the limited commercial availability and difficult synthetic access to multifunctional monomers bearing multiple, mutually reactive groups, alternative approaches such as copolymerizations of A_2 monomers with B_x comonomers ($x \geq 3$) have been developed [2–7]. Other polymerization reactions including self-condensing vinyl polymerizations initiated by cationic [8] and radical catalysts [9, 10] and ring-opening multibranching polymerizations [11–15] have been explored, mainly for the synthesis of non-conjugated hyperbranched polymers [16–18].

Hyperbranched macromolecules have been constructed from various functional groups, among which, carbon-carbon triple-bond functionality uniquely stands out because it offers ready access to hyperbranched conjugative macromolecules. Being unsaturated, it accommodates various addition reactions. In comparison to vinyl and alkyl protons, the acetylenic proton is most acidic ($pK_a = 26$; cf., $pK_a = 45$ for ethylene and $pK_a = 62$ for ethane), thus enabling facile substitution and coupling reactions. In this account, we give a brief overview of the synthesis of new hyperbranched polymers from acetylenic monomers, with an emphasis on our recent effort devoted to the development of new synthetic routes to conjugated hyperbranched polymers. Examples of their advanced functional properties are also presented.

2 Synthesis

Using acetylenic monomers carrying single and multiple triple bonds, a variety of new hyperbranched polymers with unique structures and novel properties have been synthesized by the alkyne polymerization reactions such as polycoupling, polyhydrosilylation, polycycloaddition, and polycyclotrimerization initiated by transition-metal catalysts (e.g., tantalum halides) and non-metallic species (e.g., secondary amines). Through molecular structural design and reaction condition optimization, hyperbranched polymers with high molecular weights and ready macroscopic processability have been obtained in high yields.

2.1 Polycoupling

Homo- and cross-couplings of alkyne promoted by metallic catalysts are versatile reactions for carbon-carbon bond formation and have been utilized to synthesize functional hyperbranched polymers.

2.1.1 Palladium-Catalyzed Polycoupling

Repetitive coupling of acetylenes with aryl halides is an effective way to directly build hyperbranched architecture in a stepwise manner. This type of polycoupling is often catalyzed by palladium complexes in the presence of amines and has been widely used for the preparation of well-defined oligomers, linear polymers, and perfectly branched dendrimers [19, 20].

Employing this reaction protocol, *hb*-PAEs, particularly *hb*-PPEs, have been prepared. Diiodophenylacetylene (**1**) represents a typical AB_2-type building block in this approach (Scheme 1). Palladium-catalyzed polycoupling of **1** furnished an *hb*-PPE with a bimodal SEC elution profile, charac-

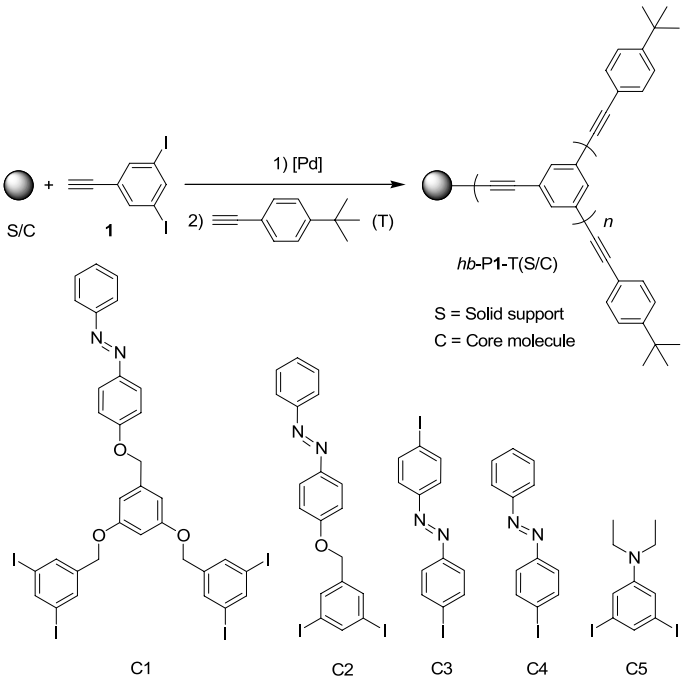

Scheme 1 Synthesis of *hb*-PPEs on a solid support (S), in the presence of core (C) molecules, and/or by the addition of a non-halogenated arylethyne terminator (T)

terized by a relatively narrow peak at the very high molecular weight region along with a long tail extending to the low molecular weight region [21]. In contrast, the *hb*-PPE obtained from the solid-supported polymerization under similar conditions possessed monomodal, narrow MWD or small PDI (M_w/M_n = 1.3). The propagation reaction could be controlled by changing the nature of the support (e.g. cross-linking density and loading) to a certain extent.

Slow addition of **1** to the solutions of multifunctional core molecules (C1–C5) resulted in higher molecular weight *hb*-PPEs with again small PDI values [22]. Control over the molecular weight was achieved by varying the monomer/core ratio. The PDI values of the *hb*-PPEs were found to decrease with increasing the degree of polymerization and with increasing the number of functional groups of the core molecule.

The Pd-polycoupling protocol works for other monomers of similar structures. For example, an AB_2-type monomer containing a 1,3,5-triazine moiety (**2**) was successfully converted into an *hb*-PAE (Scheme 2), although the resulting *hb*-P**2** was structurally irregular due to the formation of diacetylene branches in the polycoupling reaction [23]. Another example is the synthesis of a luminescent hyperbranched polymer from the polycoupling of β,β-dibromo-4-ethynylstyrene **3** (Scheme 3) [24]. Although the resulting *hb*-P**3** was only partially soluble, the structure could be elucidated by spectroscopic methods with the aid of a model compound. Theoretical calculations revealed a partially disrupted conjugation structure due to the twist of the benzene rings.

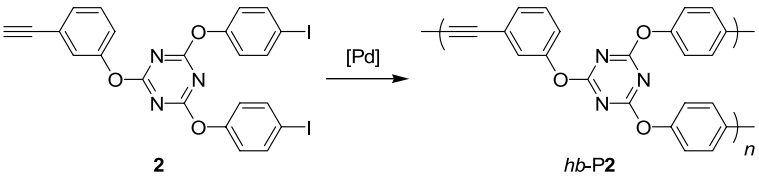

Scheme 2 Synthesis of an *hb*-PAE containing a triazine core

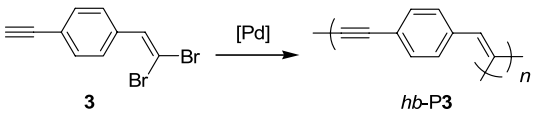

Scheme 3 Synthesis of hyperbranched polymer from β,β-dibromo-4-ethynylstyrene

Putting both halide and acetylene functionalities into a single AB_2 monomer is not a trivial job due to the involved synthetic difficulty and problems such as the formation of isomeric mixtures and undesired self-oligomerization. Purification of the desired monomers is often troublesome

and ends with low isolation yields. Separating halide and acetylene groups into two different molecules allows easier synthetic access and offers a greater variety of monomer choices but meanwhile invites the risk of cross-linking reactions. Control of the polycoupling conditions is thus a necessity if one intends to synthesize soluble hyperbranched polymers with desired structures and properties.

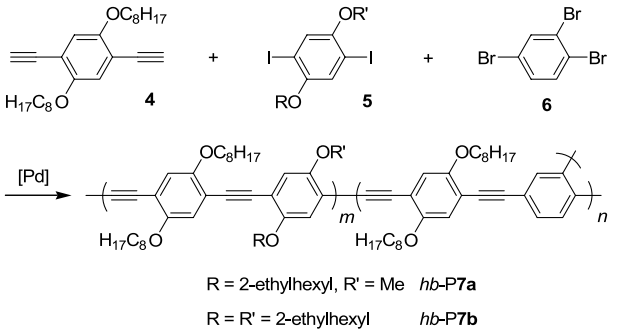

Scheme 4 Formation of cross-linked particles in the polymerization of $A_2 + B_2 + B_3$ monomers

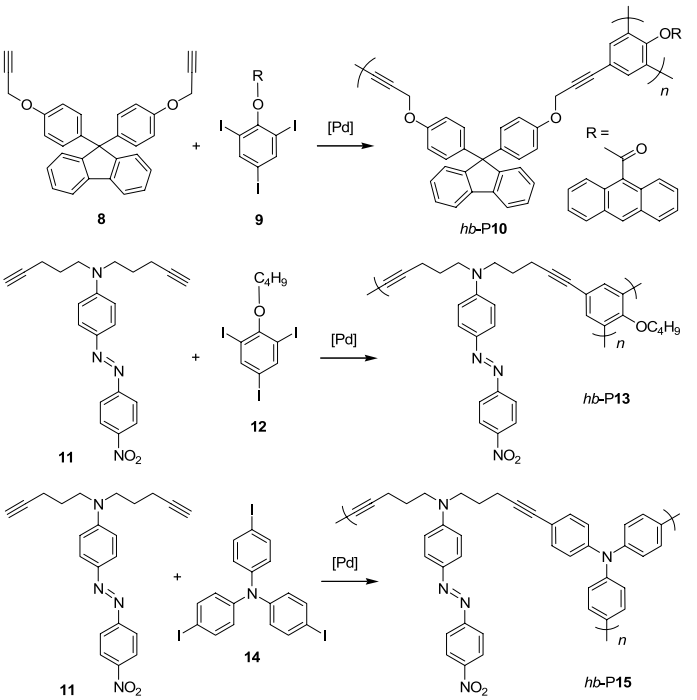

Scheme 5 $A_2 + B_3$ approach toward soluble, functional *hb*-PAEs

Cross-linking reactions readily occurred in the polymerizations of A_2 + B_2 + B_3 monomers in aqueous emulsions (Scheme 4) [25, 26]. The size of the cross-linked particles was dependant on the polymerization conditions. Micrometer-sized particles were formed when the reaction was carried out in a water–toluene–diisopropylamine mixture, whereas smaller nanoparticles were formed when the reaction was conducted in an ultrasonic bath.

We tried to optimize the polycoupling conditions by varying such parameters as polymerization time, monomer concentration and monomer addition mode, in an effort to control the polymer formation and to render the polymers soluble and processable. The optimization worked well and our A_2 + B_3 approach offered ready access to a soluble *hb*-PAE containing luminescent anthracene and fluorene chromophores (Scheme 5) [27]. Similarly, soluble azo-functionalized polymers *hb*-P**13** and *hb*-P**15** were obtained from the palladium-catalyzed polycoupling of triiodoarenes (**12** and **14**) with a diethynylazobenzene (**11**) [28].

2.1.2 Mechanistic Considerations

The overall reactions for the formation of *hb*-PAEs via Pd-catalyzed coupling are depicted in Scheme 6. As discussed above, two synthetic strategies are currently employed. The first one utilizes AB_2-type monomers, building up hyperbranched architecture through repetitive coupling of the triple bond with aryl halide. If no side reactions occur, this protocol allows only one single internal cyclization of an aryl halide with the focal acetylene unit, thus yielding *hb*-PAEs without any cross-link points. On the other hand, this internal ring closure leads to the formation of various polymeric species with different propagation possibilities, which are the cause for an increased MWD at higher conversions. Terminating the focal unit by core molecules can nicely overcome this problem (cf., Scheme 1) or even reverse the trend: with an increase in the conversion, the MWD becomes narrower [21, 22].

The second method separates the functional groups into two monomers, which facilitates synthetic work and offers greater choices to monomeric structure. In the first step, A_2 and B_3 monomers couple together to form an AB_2-type dimer that continues to react to form the hyperbranched architecture (Scheme 6). This is the case, only if the molar ratio of A_2 to B_3 is 1 : 1 and the initiation is considerably faster than the propagation [29]. It becomes immediately clear that the resultant structure is highly dependant on the type of monomers and the polymerization conditions. For the latter, it has been found that the mode of monomer addition plays a crucial role. Whereas the addition of a B_3 monomer into a solution of A_2 yields insoluble polymer gel, the opposite addition mode furnishes hyperbranched polymers with excellent solubility [30].

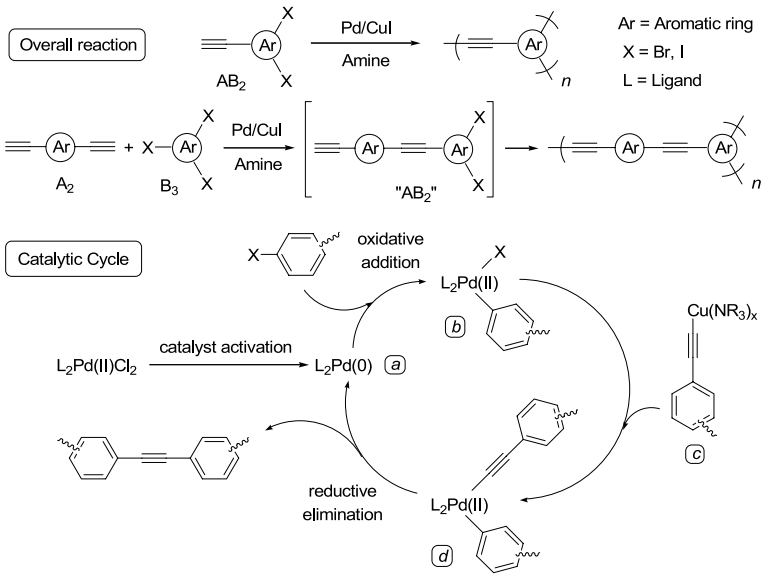

Scheme 6 Mechanisms for Pd-catalyzed polycoupling reactions

The catalytic cycle for the Pd-catalyzed polycoupling is shown in the lower panel of Scheme 6. In many cases, Pd(II) complexes such as the commercially available $(Ph_3P)_2PdCl_2$ are used as the catalytic source of Pd. In the first step, the Pd(II) is activated by cuprated alkynes (such as *c*) under reductive butadiyne elimination, creating the active catalytic species *a*. Oxidative addition of the aromatic halide produces intermediate *b*, which after transmetalation with *c* gives diorganopalladium species *d*. This species undergoes reductive elimination to finish the coupling cycle and re-forms the active catalyst *a* [31].

2.1.3 Copper-Catalyzed Polycoupling

Acetylene triple bonds react with not only aryl halides but also transition-metal complexes. An example is shown in Scheme 7, where 1,3,5-triethynylbenzene is functionalized by two equivalents of $Pt(PBu_3)Cl_2$ to form an organometallic AB_2-type monomer (**16**). Self-polycoupling of **16** initiated by a copper(I) catalyst yielded hyperbranched polymer *hb*-P**16**, which was soluble in common organic solvents and could be fully characterized by spectroscopic and chromatographic methods including SEC [32]. Cross-polycoupling between a Pt complex and an organic triyne via $A_2 + B_3$ protocol resulted in the formation of a product that was insoluble in common solvents. Only with the addition of a very large excess (e.g., 50 fold) of 1,4-diethynylbenzene, could the involved cross-linking reactions be depressed [33].

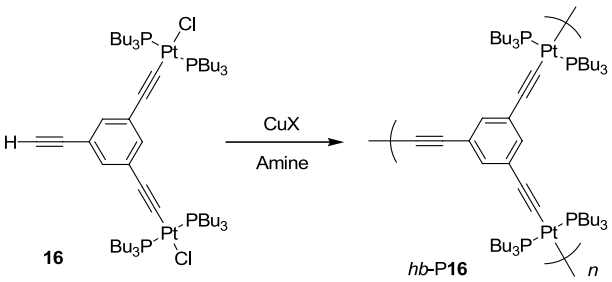

Scheme 7 Synthesis of hyperbranched organometallic polymer from AB_2-type monomer

Using aromatic triynes $Ar(C \equiv CH)_3$ as monomeric building blocks, *hb*-PYs can be readily constructed (Scheme 8) [34]. The fast polycoupling reaction could be controlled by terminating the propagating species before the

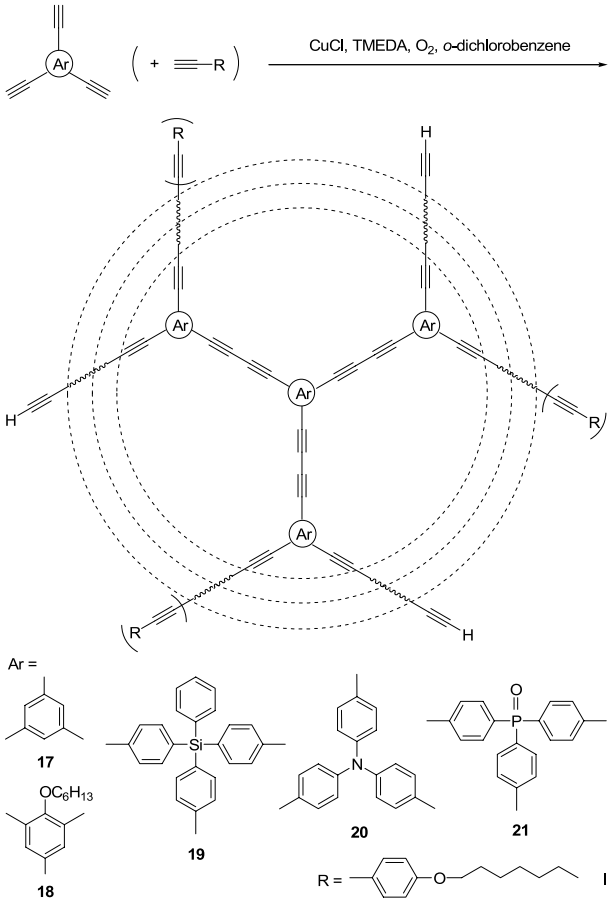

Scheme 8 Synthesis of *hb*-PYs through (co)polycoupling of triynes (with monoynes)

gel point by simply pouring the reaction mixture into acidified methanol. Soluble, high molecular weight *hb*-PYs of triynes like **17** and **19**, whose Cu-catalyzed homopolycoupling proceeded very fast, could be obtained by their copolycoupling with monoynes such as I.

In the polycoupling reactions, the formation of the diyne units proceeded via a Glaser–Hay oxidative coupling route [35–38]. Despite its wide applications in the preparation of small molecules and linear polymers containing diyne moieties, its mechanism remains unclear [38–40]. It has been proposed that a dimeric copper acetylide complex is involved, whose collapse leads to the formation of the diyne product (Scheme 9).

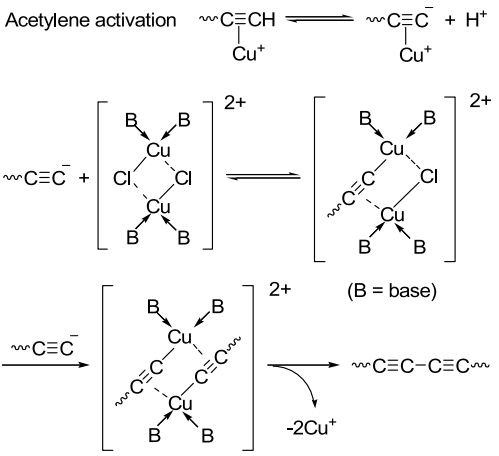

Scheme 9 Acetylene activation via π-complexation with copper(I) and proposed mechanism for the formation of diacetylene bond via cuprated alkyne dimers

Because of the one-step polymerization procedure, hyperbranched polymers often contain not only *D* and *T* but also *L* repeating units. This can be expressed by DB, which is an important structural parameter of hyperbranched polymers. DB is estimated as the sum of the *D* and *T* units divided by the sum of all the three structural units, that is, *D*, *T* and *L* [41]. By definition, a linear polymer has no dendritic units and its DB is zero, while a perfect dendrimer has no linear units and its DB is thus unity. Frey has pointed out that DB statistically approaches 0.5 in the case of polymerization of AB_2 monomers, provided that all the functional groups possess the same reactivity [42]. The structures of the *hb*-PYs could be analyzed by spectroscopic methods such as NMR and FTIR. The DB value of the phosphorous-containing polymer *hb*-P**21**, for example, was estimated to be 53% from its ^{31}P NMR chemical shifts (Chart 1).

The spectroscopic analyses revealed that both the homo- and copolyynes contained terminal triple bonds, which offers a nice opportunity to decorate

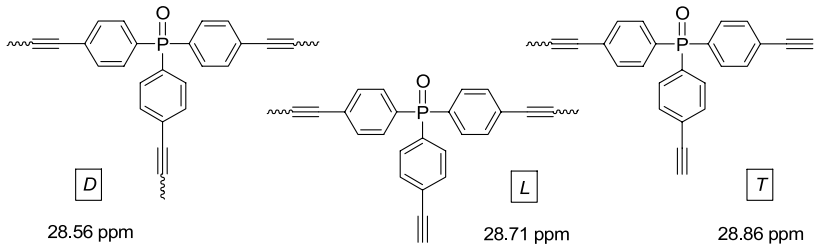

Chart 1 Structures of dendrtic (*D*), linear (*L*) and terminal (*T*) units in *hb*-P**21** and their ^{31}P NMR chemical shifts

the peripheries of the polymers by end-capping reactions. This is demonstrated by the coupling of *hb*-P**20** with aryl iodides II and III (Scheme 10). The polymer capped by phenyl iodide (*hb*-P**20**-II) became partially soluble after purification, possibly due to the π–π stacking-induced supramolecular aggregation during the precipitation and drying processes. Product *hb*-P**20**-III was soluble, thanks to the long dodecyloxy group of the end-capping agent. No signal of terminal acetylene resonance was observed in its ^{1}H NMR spectrum, unambiguously confirming the completion of the end-capping reaction.

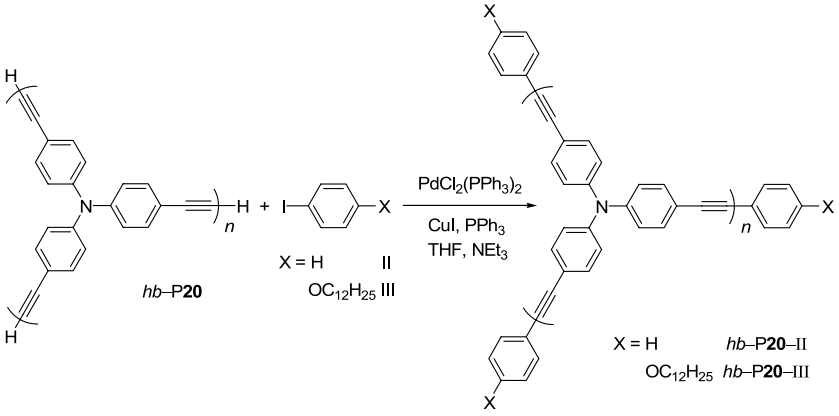

Scheme 10 End-capping reactions of *hb*-P**20**

2.2 Polyhydrosilylation

Similar to olefins, acetylenes undergo facile addition reactions. Transition metal-catalyzed hydrosilylation is such a reaction that has been utilized for the synthesis of silicon-containing hyperbranched polymers.

2.2.1
Platinum-Catalyzed Polyhydrosilylation

A hyperbranched polycarbosilane (*hb*-P**22**) was prepared by platinum-catalyzed polyhydrosilylation of methyldiethynylsilane **22** (Scheme 11) [43]. The tacky, highly soluble and stable polymer underwent thermo- and photo-induced cross-linking reactions through the peripheral ethynyl groups.

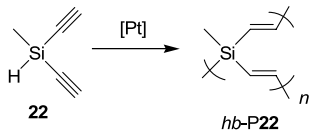

Scheme 11 Synthesis of hyperbranched polycarbosilane via polyhydrosilylation

2.2.2
Rhodium- and Palladium-Catalyzed Polyhydrosilylation

Regio- and stereoregular σ–π-conjugated hyperbranched polymers were prepared from rhodium-catalyzed polyhydrosilylation of AB_2-type silane monomers **23** and **24** (Scheme 12) [44, 45]. Polymer *hb*-P**23** contained 95% trans vinylene units and lost merely 9% of its weight when heated under nitrogen to a temperature as high as 900 °C. It showed a UV absorption peak at $\sim$ 275 nm due to the π–π^* transition and a weak absorption at $\sim$ 330 nm due to the π–to–σ charge transfer, which was hardly seen in its linear polymer congeners.

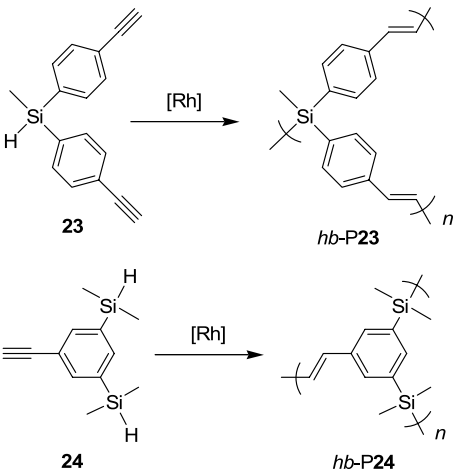

Scheme 12 Synthesis of σ–π conjugated hyperbranched polymers through rhodium-catalyzed polyhydrosilylation

The unreacted peripheral silane groups of *hb*-P**24** could either be terminated by reacting with an excess amount of phenylacetylene or cross-linked by hydrolysis and aerial oxidation. Whereas the first reaction gave a soluble hyperbranched polymer, the latter furnished a transparent gel via siloxane linkages without any obvious defects such as phase separation and decomposition. The gel exhibited a strong resistance against various organic solvents, showed a weak absorption at above 300 nm due to the involved charge transfer, and emitted an intense blue light.

In a similar approach, palladium-catalyzed polyhydrosilylation afforded soluble hyperbranched poly(silylenedivinylene)s through an $A_2 + B_2 + B_3$ protocol with 1,3,5-triethynylbenzene and *B*,*B*′,*B*″-triethynyl-*N*,*N*′,*N*″-trimethylborazine as the branching units [46]. The resultant polymers showed higher thermal stabilities and higher char yields than their linear analogs. The hyperbranched polymers obtained from 1,3,5-triethynylbenzene showed intensified broad UV absorptions and enhanced light emissions.

2.3 Polycycloaddition

Polycycloaddition reactions of acetylenic monomers have been used to synthesize hyperbranched polymers comprised of pure aromatic rings and heterocyclic units.

2.3.1 Diels–Alder Polycycloaddition

Müllen and coworkers utilized the Diels–Alder reaction to prepare *hb*-PPs (*hb*-P**25** to *hb*-P**27**) with M_w up to 107 000 from ethynyl-, propynyl-, and phenylethynyl-substituted tetraphenylcyclopentadienones (Scheme 13) [47]. Despite their high molecular weights and rigid phenyl rings, all the polymers showed good solubility in common aromatic solvents such as toluene and benzene.

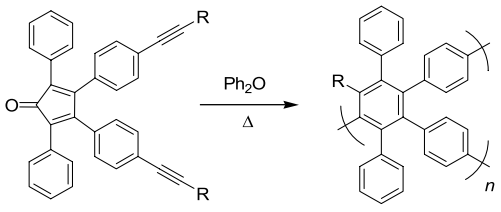

Scheme 13 Synthesis of *hb*-PPs via Diels–Alder polycycloaddition

2.3.2
1,3-Dipolar Polycycloaddition (Click Polymerization)

The formation of triazole rings by the reactions of azides and acetylenes was first described by Huisgen and coworkers [48, 49] and has recently been promoted as "click" chemistry by Sharpless et al. [50, 51]. This versatile [3 + 2] dipolar cycloaddition proved to be useful for the synthesis of hyperbranched polytriazoles via 1,3-dipolar polycycloaddition of AB_2-type monomers **28** and **29** (Scheme 14) [52]. The monomers exhibited very high reactivity: the

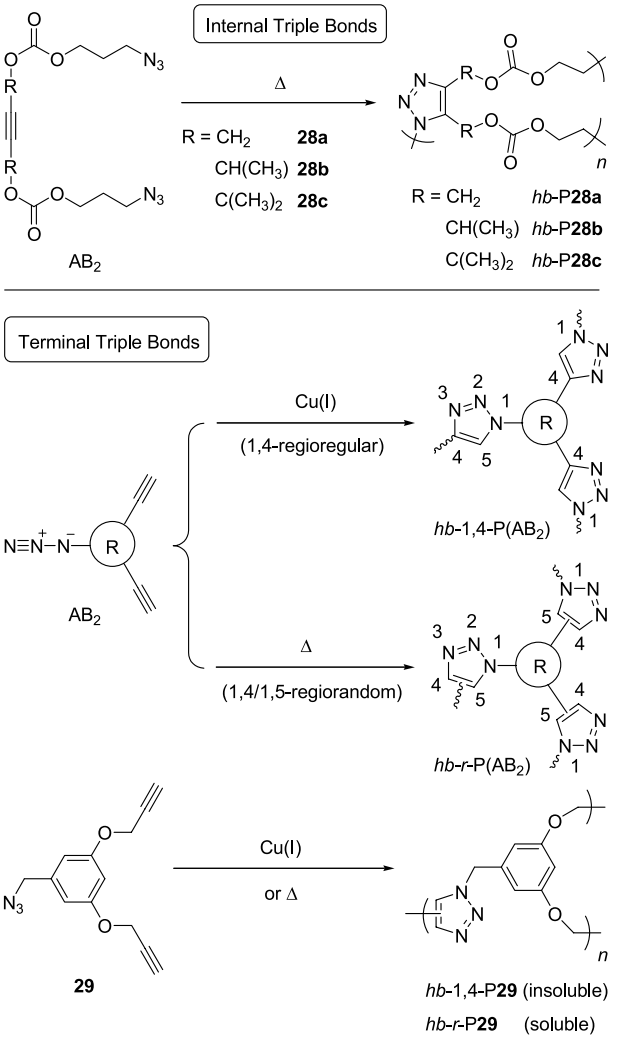

Scheme 14 Synthesis of *hb*-PTAs by "click" polymerization from AB_2-type monomers

low temperature auto-polymerization transformed them into soluble, high molecular weight *hb*-PTAs with an estimated DB value of 50%. Copper(I)-catalyzed polycycloaddition of **29** furnished a 1,4-stereoregular *hb*-1,4-P**29**, however, with intractability.

This study demonstrated the potential of the [3 + 2] polycycloaddition reaction involving azides and alkynes for the preparation of new hyperbranched polymers and meanwhile showed the necessity of controlling the polymerization conditions because of the high reactivity of the azide and alkyne functionalities [53]. One possibility to gain control and to inhibit autopolymerization of the monomers is to put the functional groups in two separate monomers. This would make it easier to synthesize and purify the monomers and make it possible to extend the shelf-life of the monomers. Thermally induced 1,3-dipolar polycycloaddition of diazides and triynes furnished soluble hyperbranched polytriazoles (Scheme 15 and Table 1, entries 1 and 2) [54]. Similar to the AB_2-type monomers, attempts to prepare 1,4-regioregular polytriazoles through copper(I)-mediated cycloaddi-

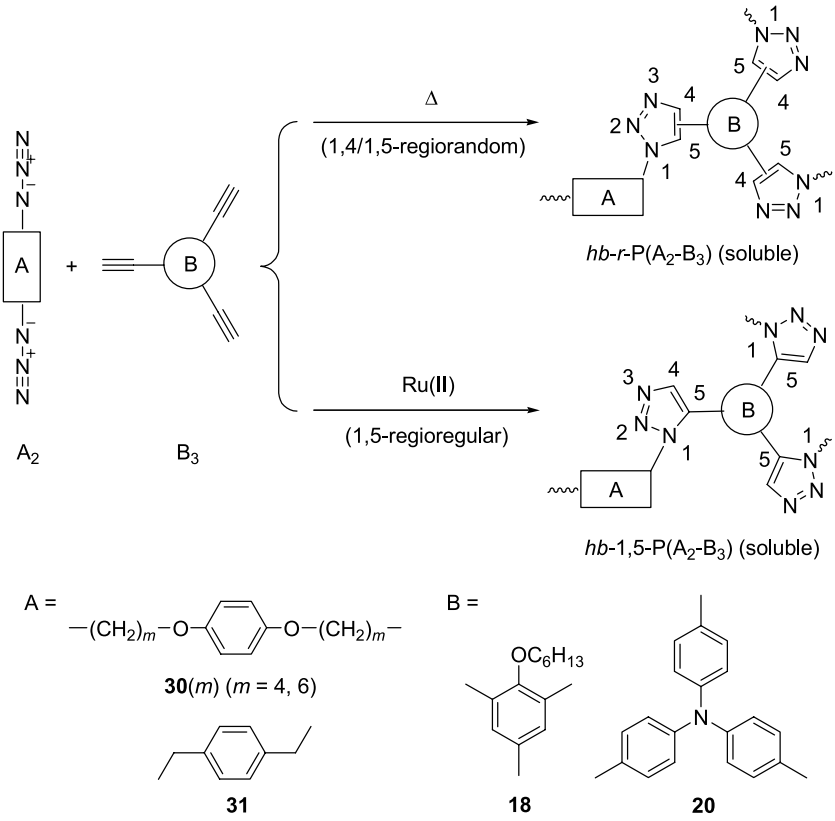

Scheme 15 *hb*-PTAs via $A_2 + B_3$ 1,3-dipolar cycloaddition

Table 1 Synthesis of hyperbranched polytriazoles

Entry	Monomers	Time (h)	Polymer	Yield (%)	M_w [a]	PDI [a]
Thermally Initiated Polymerization [b]						
1	**30**(4) + **20**	72	*hb-r*-P**30**(4)-**20**	64.0	5500	2.0
2	**30**(6) + **20**	72	*hb-r*-P**30**(6)-**20**	75.7	11 400	2.7
Transition Metal-Catalyzed Polymerization [b]						
3	**30**(4) + **20**	0.33	*hb-1,5*-P**30**(4)-**20**	62.5 [c]	5350	2.4
4	**30**(6) + **20**	0.50	*hb-1,5*-P**30**(6)-**20**	74.9	9370	2.7

[a] Estimated in THF by GPC on the basis of a polystyrene calibration
[b] $[\mathbf{20}]_0/[\mathbf{30}(m)]_0 = 2:3$, $[\mathbf{20}]_0 = 0.12$ M; under nitrogen in 1,4-dioxane at 101 °C (entries 1 and 2) or in THF at 60 °C using $Cp^*Ru(PPh_3)_2Cl$ as catalyst (entries 3 and 4)
[c] Soluble fraction (total yield: 84.5%)

tion resulted only in insoluble polymers. Stereoregular 1,5-substituted *hb*-PTAs, however, were successfully obtained when $Cp^*RuCl(PPh_3)_2$ was used as the catalyst. Compared to their regiorandom congeners, completely soluble polymers *hb*-1,5-P(**30**–**20**) with similar isolation yields and molecular weights were obtained in much shorter polymerization times (Table 1, entries 3 and 4). One reason for the solubility difference in the hyperbranched PTAs might be because the triazole rings function as ligands that form complexes with copper but not ruthenium ions, which thus cross-links the *hb*-1,4-PTA spheres [55]. Another possible cause might be due to the difference in the architectural structures of 1,4- and 1,5-disubstituted triazole rings. The 1,4-isomer experiences little steric interaction with the neighboring phenyl groups and can arrange in a relatively planar confirmation (Fig. 1). In contrast, its 1,5-substituted congener experiences strong steric repulsion, forcing the molecule to adopt a more twisted conformation. The structural planarity of the 1,4-isomer may facilitate π–π stacking of the aromatic moieties, leading to a lower solubility.

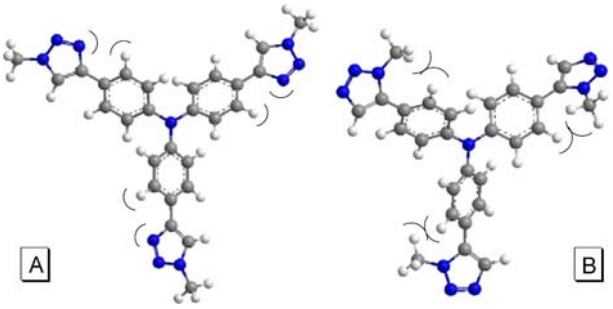

Fig. 1 Simulated conformations of **A** tris[4-(1-methyl-1*H*-1,2,3-triazol-4-yl)phenyl]amine and **B** tris[4-(1-methyl-1*H*-1,2,3-triazol-5-yl)phenyl]amine

Spectroscopic analysis revealed that the thermally initiated [3 + 2] polycycloaddition produced 1,4- and 1,5-substituted triazole isomers in an approximately 1 : 1 ratio. This ratio appears to be statistic and dependant on the bulkiness of the organic moieties. For example, *hb-r*-P[**30**(4)–**20**] with butyl spacers contained slightly more 1,4-triazole isomers than did *hb-r*-P[**30**(6)–**20**] with hexyl spacers. This becomes clearer if we look at the proposed transition states *a* and *b* of the [3 + 2]-dipolar cycloaddition (Scheme 16). Because of their molecular orbital symmetry, the acetylene and azide functional groups arrange in two parallel planes, a so-called "two-plane orientation complex" [48], which facilitates a concerted ring formation. If the monomer fragment or the polymer branch (∼∼∼) attached to the functional groups are bulky, steric repulsion will come into play and transition state *a* will be

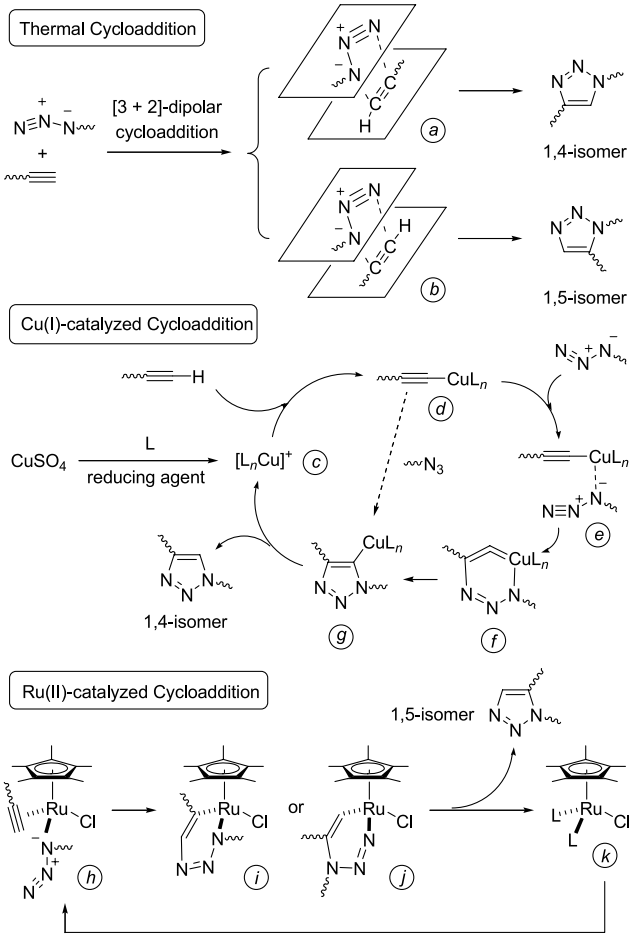

Scheme 16 Proposed mechanisms for thermal and catalytic cycloaddition reactions

favored, hence the formation of a hyperbranched polymer with a higher 1,4-isomer content. With a small steric interaction, both the two transition states are possible. As a result, the reaction gives a statistic mixture with both 1,4- and 1,5-isomeric structures.

Whilst the thermally induced 1,2,3-triazole formation between acetylene and azide yields a mixture of 1,4 and 1,5-isomers, stereoregularity can be achieved when the cycloaddition is catalyzed by a copper(I) salt (Scheme 16). The active catalytic species (*c*) is usually generated from a copper(II) salt in the presence of a reducing agent such as ascorbic acid or sodium ascorbate. The catalytic cycle commences with the generation of copper(I) acetylide (*d*). Density functional theory calculations show that a concerted cycloaddition directly from *d* to *g* is disfavored by $\sim 12-15\,\text{kcal mol}^{-1}$ and that the cycloaddition proceeds in a stepwise annealing sequence ($d \rightarrow e \rightarrow f \rightarrow g$), going through the intriguing species of six-membered metallocycle *f* [56]. As mentioned above, so far there has been no report in the literature utilizing this potential protocol to synthesize soluble 1,4-regioregular PTAs and the attempts made by others and us had all been unsuccessful. The mechanism of the ruthenium(II)-catalyzed synthesis of 1,5-substituted *hb*-1,5-PTAs is not well understood at present and needs more detailed investigations. The 1,5-disubstituted 1,2,3-triazole rings may have formed via an initial oxidative coupling of the alkyne and azide groups on the ruthenium metal center, followed by reductive elimination of the 1,5-isomeric unit from the six-membered ruthenacycles *i* and/or *j* (Scheme 16) [57]. The ruthenium(II) catalyst is also active for internal alkynes, forming 1,4,5-trisubstituted 1,2,3-triazoles in a regioselective manner [58]. This new protocol will help generate stereoregular trisubstituted *hb*-PTAs.

2.4 Polycyclotrimerization

All the hyperbranched polymers prepared by the synthetic routes discussed above have one feature in common: their branching units are already embedded in their monomer building blocks. In other words, nonlinear monomers with trifunctional groups are needed in order to construct the hyperbranched macromolecules. It is of great interest to develop new polymerization processes, where the propagation reaction inherently generates branching structures from simple, linear monomers. An example of such a reaction is transition metal-catalyzed polycyclotrimerization of diynes (Scheme 17). This kind of [2 + 2 + 2] cyclization reaction involves a single monomer species, suffers no stoichiometric constraint, and can potentially produce polymers with high molecular weights and high stability. Inherently the resultant polymers should be highly branched, because the polycyclotrimerization mechanism is intolerant of, or incompatible with, the formation of linear repeat units inside the hyperbranched cores.

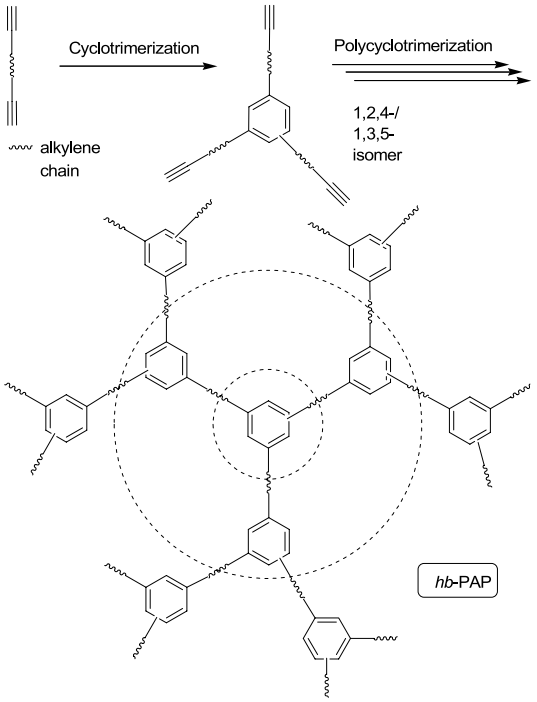

Scheme 17 Synthesis of hyperbranched polymer through diyne polycyclotrimerization

A few research groups had looked into the possibility of utilizing the alkyne cyclization for polymer synthesis in the early 1970s and late 1980s [59–63]. But as summarized by Sergeyev et al. in a symposium review article [59] at that time, the resultant homopolymers "are infusible and insoluble in conventional organic solvents" and "are difficult to reprocess into manufactured articles". The interest in the alkyne homopolycyclotrimerization had therefore subsided, with almost nobody revisiting the subject over the past decades, because the insolubility of the homopolymers of the diynes rendered their structural characterization a difficult proposition and their intractability made them almost useless in terms of finding practical applications as plastic materials.

2.4.1 Hyperbranched Poly(alkylenephenylene)s

We have studied homopolycyclotrimerizations of aliphatic terminal diynes with various alkylene spacer lengths catalyzed by tantalum and niobium halides or by binary mixtures of the metal halides and tetraphenyltin (Scheme 18) [64–66]. Under optimized conditions, completely soluble diyne homopolymers with high molecular weights (M_w up to $\sim 1.4 \times 10^6$) and pre-

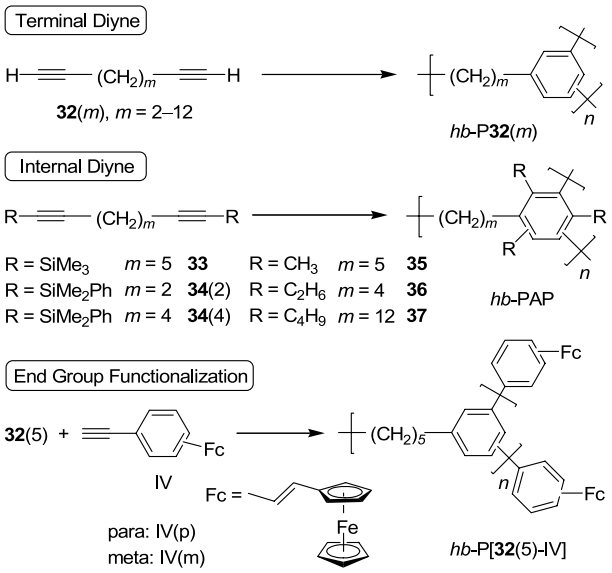

Scheme 18 Homopolycyclotrimerizations of terminal and internal diynes and synthesis of *hb*-PAPs with functional end groups

dominant 1,2,4-benzenetriyl core structures were obtained in high yields (up to 93%). Internal diynes could also be polymerized into hexasubstituted *hb*-PAPs [67]. Copolycyclotrimerization of the aliphatic diynes with monoynes enabled the incorporation of functional groups into the *hb*-PAP structure at the molecular level. This was demonstrated by the synthesis of *hb*-P[**32**(5)-IV]: the *hb*-PAP was decorated by redox-active ferrocene units on its periphery [68].

The alkyne cyclotrimerizations catalyzed by the complexes of late transition metals such as Ni, Zn, Rh, Pd, Ru, Co, Ir, etc. have been extensively studied and the involved reaction mechanisms have been well established [69–76]. Although the acetylene cyclotrimerizations catalyzed by the complexes of early transition metals have been less studied, highly regioselective systems have been developed [77–79]. For example, some titanium complexes have been found to catalyze the regioselective cyclotrimerizations of terminal alkynes in high efficiencies, giving 1,2,4-trisubstituted benzenes in excellent regioselectivities (≥97%) and isolation yields (≥95%) [77]. Group V transition metal complexes such as niobium and tantalum halides usually work very well and produce *hb*-PAPs with predominately 1,2,4-substituted benzenes. It has been proposed that tantallacyclic intermediates are involved in tantalum-catalyzed alkyne cyclotrimerizations [80–83]. The diyne polycyclotrimerization may have followed similar paths with the metallacyclic intermediates serving as the initiating and propagating species. An in-situ generated Ta(III) species [84, 85] may oxidatively add to a diyne (*a*) to form

a tantallacyclopropene intermediate *b* (Scheme 19). Insertion of a triple bond of another diyne monomer to *b* gives three possible regioisomers of tantallacyclopentadienes *c*, among which c_I experiences the least steric repulsion from ligands R and may thus be preferentially formed. Addition of a third diyne to c_I can potentially form two tantallacycloheptatriene isomers (*d*) and two Diels–Alder adducts of tantallanorbornadienes (*e*). Each of the intermediates experiences different steric interactions but all of them give the same product of 1,2,4-trisubstituted benzene *f* through reductive elimination of the metal species. Following a similar pathway, 1,3,5-substituted benzene unit *g* may be generated from tantallacyclopentadiene c_{II}. The 1,2,4- and 1,3,5-arenes *f* and *g* formed during the initiation step will serve as propagating species to follow the same reaction pathway to grow to a higher generation. Iterative repeats of the oxidative addition–reductive elimination cycles in the propagation step eventually lead to the formation of an *hb*-PAP.

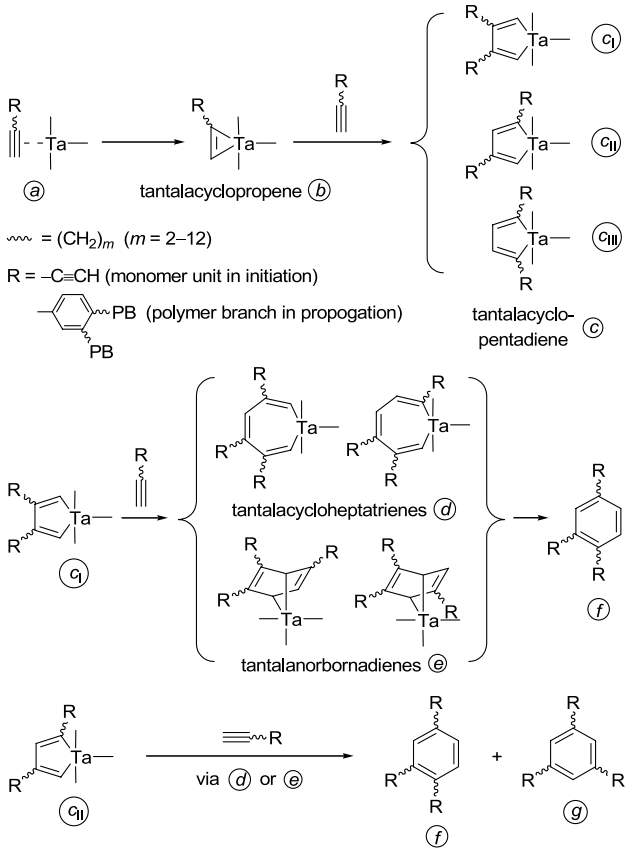

Scheme 19 Proposed mechanism for tantalum-catalyzed alkyne polycyclotrimerization

In Scheme 19, only is the possibility for one triple bond of a diyne monomer to react with a metal center considered. As outlined in Scheme 20, it is possible that through a "back-biting" reaction pathway, two triple bonds in one diyne molecule add to the same metal center to form a tantallacyclopentadiene intermediate *c*. Further reaction with another triple bond of a propagating branch would produce benzocycloalkene *f*, which will terminate the growth of the branch by end-capping it. A similar structure can be formed by the end-capping reaction of a propagating species *d* with diyne **32**(*m*). The formation of tantallacyclopentadiene followed by the back-biting of the second alkyne easily leads to the ring closure due to their close proximity. Depending on the length of alkylene spacer, 4- to 8-membered benzannulated rings may be formed as end groups on the peripheries of *hb*-PAPs.

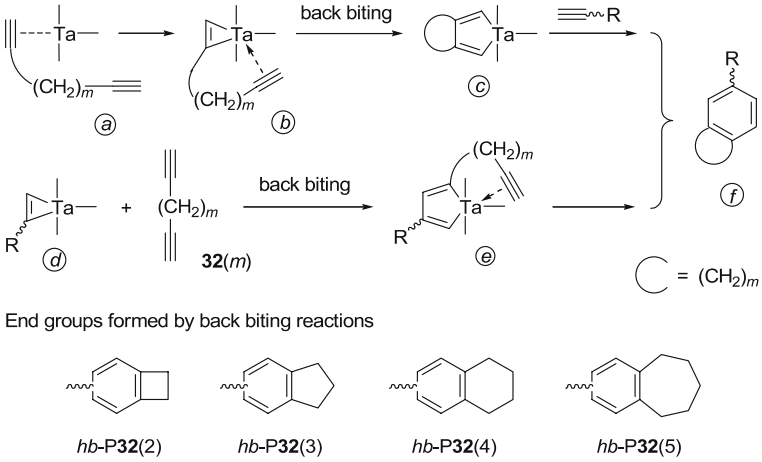

Scheme 20 Proposed mechanism for back-biting reactions occurring in polycyclotrimerization of aliphatic diynes

The back-biting reaction plays an important role in the polycyclotrimerization of the aliphatic diynes. If this end-capping reaction is too active, the propagating branches will be easily terminated, giving only oligomeric products. On the other hand, if the back-biting reaction is too sluggish, the polymerization will become difficult to control, resulting in the formation of cross-linked gels. Fine tuning the back-biting reaction will help control the formation of the reaction products. For example, diynes with two and three short methylene spacers such as **32**(2) and **32**(3), respectively, have a high tendency towards back-biting and thus form *hb*-PAPs of low molecular weights (Table 2, nos. 1 and 2). No terminal triple bonds but strong back-biting signals can be observed in their ^{1}H NMR analyses. Diynes with long spacers [**32**(*m*), $m \geq 6$] show low back-biting activity, which can be easily confirmed by the existence of their unterminated triple bonds. As a result, the polymer-

Table 2 Analysis of the products [*hb*-P**32**(*m*)] obtained from the polycyclotrimerizations of aliphatic diynes **32**(*m*) with different lengths (*m*) of methylene spacers[a]

No.	Spacer	Solubility[b]	Triple bond[c]	Back biting[d]	M_w[e]	M_w/M_n[e]
1	$-(CH_2)_2-$	Soluble	Not observed	Strong	~ 3000	2.3
2	$-(CH_2)_3-$	Soluble	Not observed	Very strong	~ 900	1.5
3	$-(CH_2)_4-$	Soluble	Observed	Medium	~ 60 000	4.9
4	$-(CH_2)_5-$	Soluble	Not observed	Medium	~ 40 000	5.0
5	$-(CH_2)_6-$	Soluble	Observed	Very weak	~ 600 000	23.0
6	$-(CH_2)_8-$	Insoluble				
7	$-(CH_2)_9-$	Soluble	Observed	Weak	~ 200 000	7.9
8	$-(CH_2)_{10}-$	Insoluble				

[a] The polymerization reactions were carried out in toluene at room temperature under nitrogen by using $TaCl_5 - Ph_4Sn$ as catalyst
[b] Tested at room temperature in common organic solvents including toluene, benzene, chloroform, DCM, and THF
[c] Signal in the ^1H NMR spectrum of *hb*-PAP
[d] Signal intensity in the ^1H NMR spectrum of *hb*-PAP
[e] Estimated by SEC in THF on the basis of a linear polystyrene calibration

izations are difficult to control, forming polymers with very high M_ws and extremely broad PDIs (Table 2, nos. 5 and 7) or even totally insoluble gels (Table 2, nos. 6 and 8).

A unique odd-even effect of the monomers in the diyne polycyclotrimerization was observed. In the aliphatic diynes with an odd number of methylene spacers, their triple bonds locate in the same side, which facilitates the back-biting reaction (Scheme 21). In contrast, in the diynes with an even number of methylene units, their triple bonds locate in the opposite sides: these unfavorable positions frustrate the back-biting reaction. Consequently, *hb*-P**32**(4) possessed triple bond residues in its final structure, whereas its congener *hb*-P**32**(5) did not.

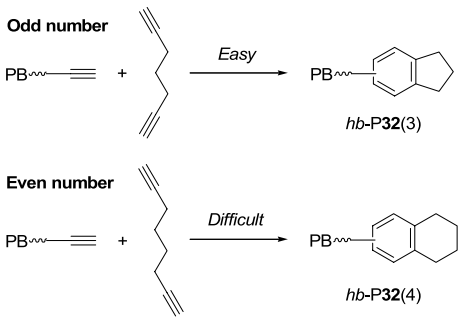

Scheme 21 Odd-even effect in the back-biting reaction

The *hb*-PAPs contain numerous branching units, resulting from the cyclization propagation and back-biting termination. In addition to the branching structures, there exist pseudo-"linear" structure in the polymers, formed by the reaction of the closely located triple bonds in a 1,2,4-substituted benzene ring (Scheme 22). The acetylene triple bonds in the 1 and 2 positions can form a new benzene ring through cyclotrimerization with another triple bond from a monomer or a polymer branch. Although this may also be considered as a "cross-linking" reaction, the structural motif is not detrimental to the solubility of *hb*-PAP due to its overall "linear" propagation mode. Combining all these three structural features, the *hb*-PAPs possess a molecular architecture similar to that of glycogen (Scheme 23), a hyperbranched biopolymer [66].

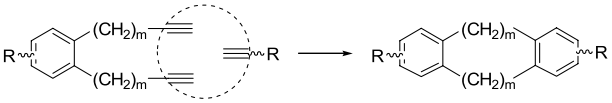

Scheme 22 Pseudo-"linear" propagation mode in the diyne polycyclotrimerization

Changing terminal diynes to internal ones changes the polymerizability of the diyne monomers as well as the structure of the resultant polymers. The attempted polymerizations of the internal diynes with such bulky groups as trimethylsilyl and dimethyl(phenyl)silyl groups either gave no polymeric products or produced oligomeric species (Table 3). Internal diynes with "slim" head groups such as Bu were active. Similar to the case of terminal diynes, if the alkyl spacer between the two triple bonds in the internal diynes was too long, the polymerizations of the monomers gave insoluble gels due to the absence of the growth-controlling back-biting termination. Only did

Table 3 Results of attempted polymerizations of internal diynes

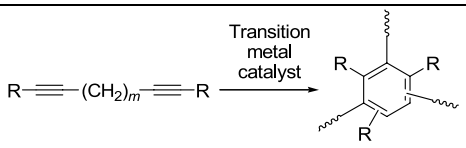

R	m	Product
– $SiMe_2Ph$	2, 4	No polymer or only oligomer
– $SiMe_3$	5	
– C_4H_9	12	Insoluble gel
– C_2H_5	4	Soluble polymer
– CH_3	5	

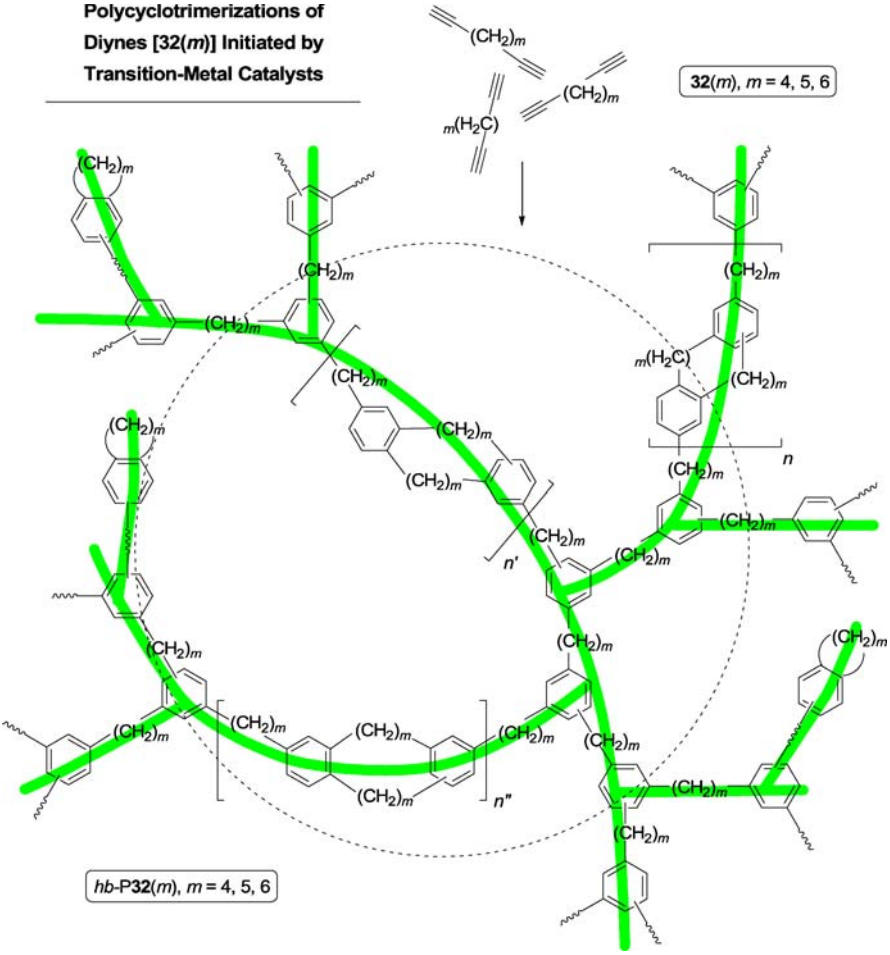

Scheme 23 Glycogen-like molecular architecture of *hb*-PAPs

those internal diynes with proper head groups and spacer lengths produce completely soluble, high molecular weight polymers.

2.4.2 Hyperbranched Polyarylenes

As discussed above, changing the diyne position from terminal to internal is one way to change the nature of the hyperbranched polymers. More profound changes can be brought about by replacing the aliphatic spacers with aryl rings. Different from the isolated benzene rings in the *hb*-PAPs, here the "new" benzene rings formed by the polycyclotrimerization help the "old" aromatic rings to interconnect into conjugated *hb*-PAs (Scheme 24).

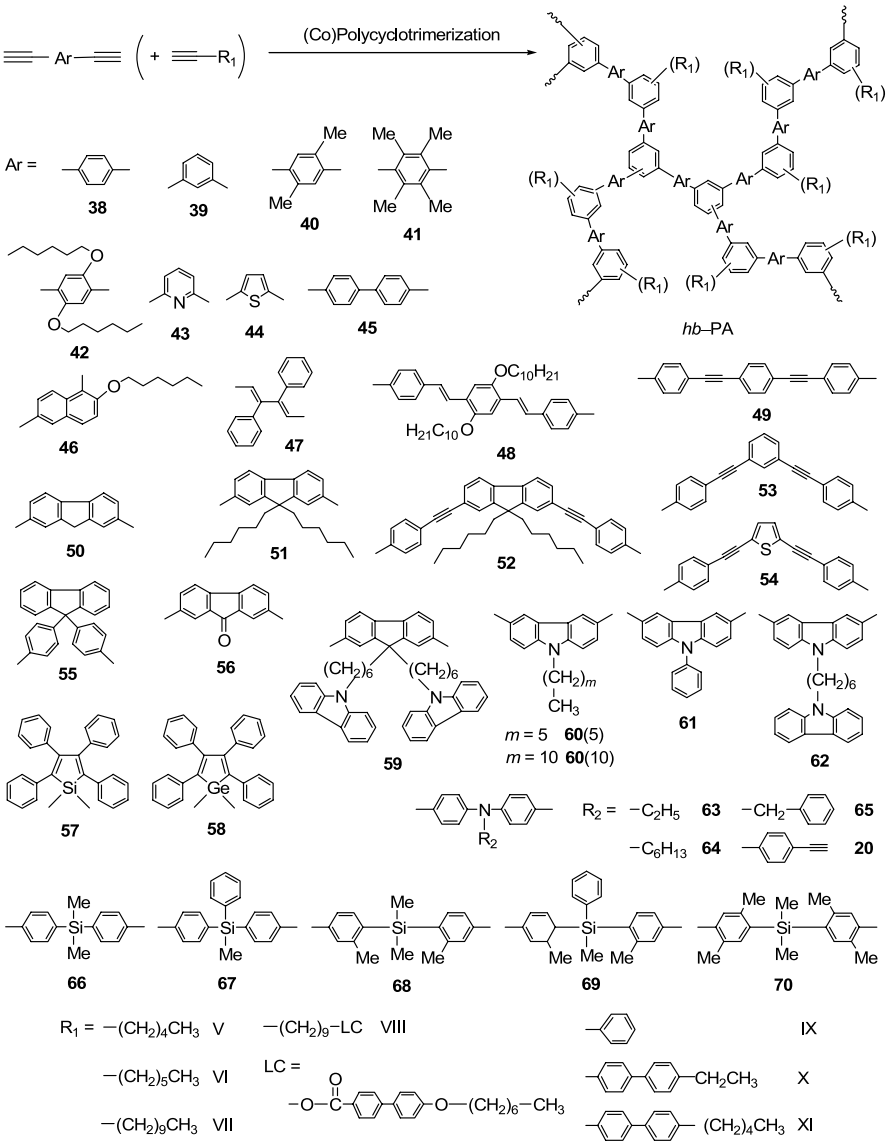

Scheme 24 Synthesis of *hb*-PAs by (co)polycyclotrimerization of aryldiynes (with monoynes)

Because of the lack of the back-biting capability of the rigid aromatic diynes, their homopolycyclotrimerizations are not as easy to control as those of their congeners of flexible aliphatic diynes. Nevertheless, high molecular weight *hb*-PAs could be obtained in quantitative yields from the homopolycyclotrimerizations of nitrogen-containing aromatic diyne (**59–65**) catalyzed by

$CpCo(CO)_2$ under UV irradiation and from the polymerizations of metallolyl (**57** and **58**) and silyldiynes (**66–70**) catalyzed by tantalum halides [86–91]. The homopolycyclotrimerizations of other aromatic diynes (**38–56**) all proceeded very rapidly, giving polymeric products that were only partially or totally insoluble in common organic solvents due to the involved cross-linking reactions. The large free volumes and irregular molecular structures generated by the nonlinear carbazolyl, diphenylamine, metallolyl and silyl groups may have helped endow the homopolymers (*hb*-P**57** to *hb*-P**70**) with the excellent solubility.

Structural analysis of the homopolymers by spectroscopic methods confirmed that the diynes had undergone [2 + 2 + 2] polycyclotrimerizations by forming new benzene rings from their acetylenic triple bonds. The ratio of the 1,2,4- to 1,3,5-isomers of the trisubstituted benzene rings was estimated to be $\sim 2.2 : 1$. Careful evaluation of the ^{1}H NMR spectra unveiled that the number of terminal triple bonds in the final *hb*-PAs was much smaller than that in an "ideal" hyperbranched structure produced by the diyne polycyclotrimerization. This result suggests that intra-sphere ring formation might have been involved in the cyclotrimerization polymerization.

To account for the "missing" acetylenic protons, three possible pathways for the consumption of the triple bonds were proposed and are depicted in Scheme 25. The first pathway is via a normal P_1M_2 growth mode, where P and M stand for polymer and monomer, respectively. The second is via an intracyclotrimerization mode of P_2M_1 type, with two triple bonds from two polymer branches and one from a monomer involved. The third is via another "pure" intracyclotrimerization mode of P_3 type, with the three triple bonds all from the branches of a polymer. The experimental results indicate that one or both of the intracyclotrimerization modes must have been at play in the polycyclotrimerization of silylenediynes. However, the newly formed benzene rings by these intracyclotrimerizations are undistinguishable from each other and are also indistinct from those formed by the normal polycyclotrimerization reactions in the NMR spectra, making it difficult to experimentally determine the probabilities of the intracyclotrimerization reactions.

To solve this problem, computational simulation was exercised. The models of the polymers were built, and the probabilities of the growth modes were estimated according to the minimized energy of the structures, using the Materials Studio program[1]. An example of the outputs of the computer simulations is shown in Fig. 2. The overall structure of *hb*-P**66** looks like a star-shaped macromolecule containing a number of small cyclic units (Fig. 2, lower right panel). The total number of the triple bonds left inside the hyperbranched structure and the total number of the aromatic protons were in agreement with the numbers estimated from the ^{1}H NMR analysis.

[1] Materials Studio is a software environment that brings together the world's most advanced materials simulation and informatics technology. It is a product of Accelrys Inc.

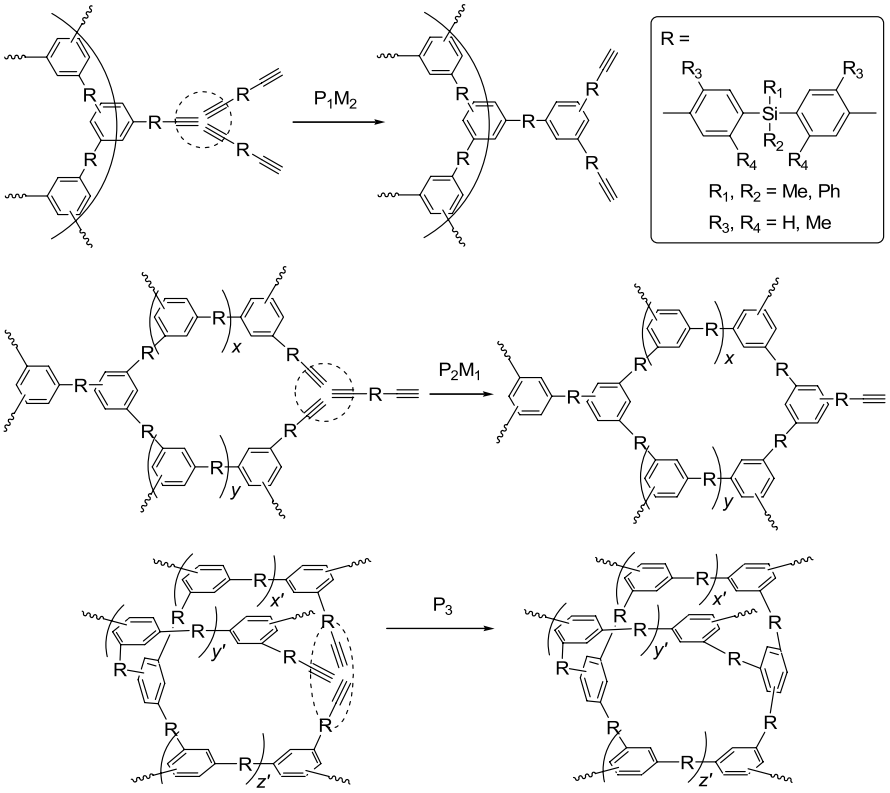

Scheme 25 Propagation modes for the homopolycyclotrimerization of silyldiynes

The computer simulation model is thus consistent with the structure of the real polymer. Estimation of the three different growth modes gave possibilities of 64%, 34% and 2% for the P_1M_2, P_2M_1 and P_3 modes, respectively. Although more than 1/3 (or 36%) of the propagation modes are via the intracyclotrimerization reactions, most of the cycles are small, being formed by only two monomer units mainly due to the close proximity of the 1 and 2 positions of the newly formed 1,2,4-trisubstituted benzenes. The small rings are strung together like beads in a necklace. This structure model is in agreement with the excellent solubility of the polymer, although it contains numerous cyclic structures.

As mentioned above, the homopolycyclotrimerization was limited to a small number of diynes in terms of generation of soluble polymers. To overcome the problem of uncontrolled cross-linking reactions and to improve the solubility of the polymers, copolycyclotrimerizations of aromatic diynes with monoynes (V–XI) were carried out (cf., Scheme 24). This approach worked very well: all the copolycyclotrimerization reactions proceeded smoothly with good controllability, producing completely soluble hyperbranched copoly-

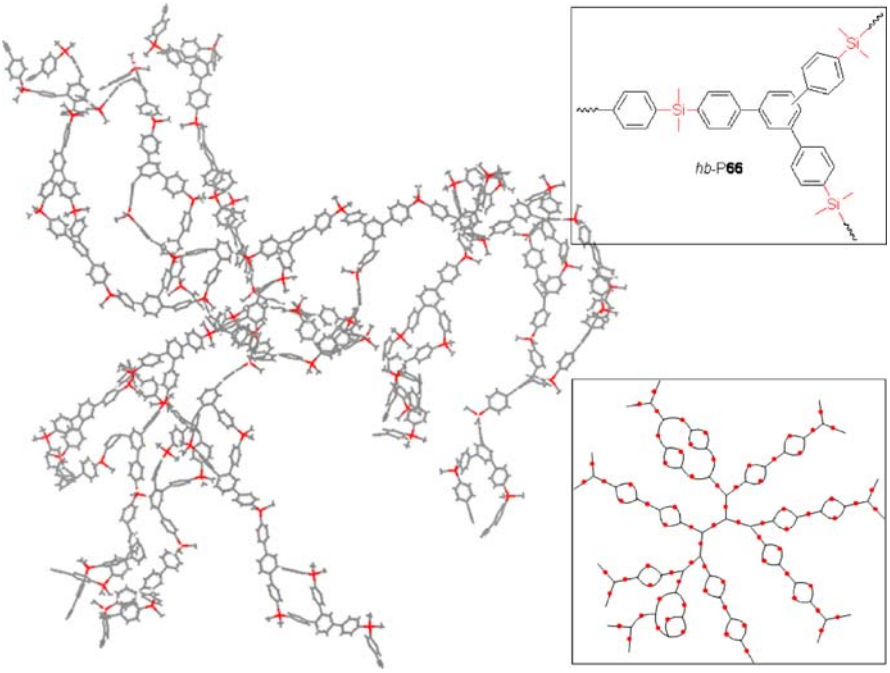

Fig. 2 Three-dimensional macromolecular structure of *hb*-P**66** simulated by Materials Studio program. *Inset*: Chemical structure of *hb*-P**66** (*upper panel*) and simplified illustration of the two-dimensional geometric structure of *hb*-P**66** (*lower panel*)

arylenes with high molecular weights (M_w up to $\sim 1.8 \times 10^5$) in high isolation yields (up to 99.7%) [88, 92–98]. 1-Alkynes (V–VIII) are generally better comonomers than 1-arylacetylenes (IX–XI) when the molecular weights of the *hb*-PAs are concerned. This is probably due to two effects. First, the long alkyl chains may confer higher solubility on the propagating species, therefore enabling their continued, further growth into bigger polymers. The second might be associated with an electronic effect. The electron-donating alkyl groups make the triple bonds of 1-alkynes electronically richer, which are likely to favorably interact with the electron-poorer aromatic diynes [99], hence promoting the formation of high molecular weight *hb*-PAs.

As a nice example, a "true" *hb*-PP without any substituent groups (or a "pure", all-aromatic plastic) was readily synthesized by the copoly-cyclotrimerization of diethynylbenzene (**38**) with phenylacetylene (IX) (Scheme 26). Whilst its cousin of linear PPP becomes insoluble and intractable when the molecular weight of PPP reaches just a few thousands, the highly branched and irregular molecular structure of *hb*-P(**38**-X) hampers strong π–π stacking of the aromatic rings, making the polymer completely soluble in common organic solvents.

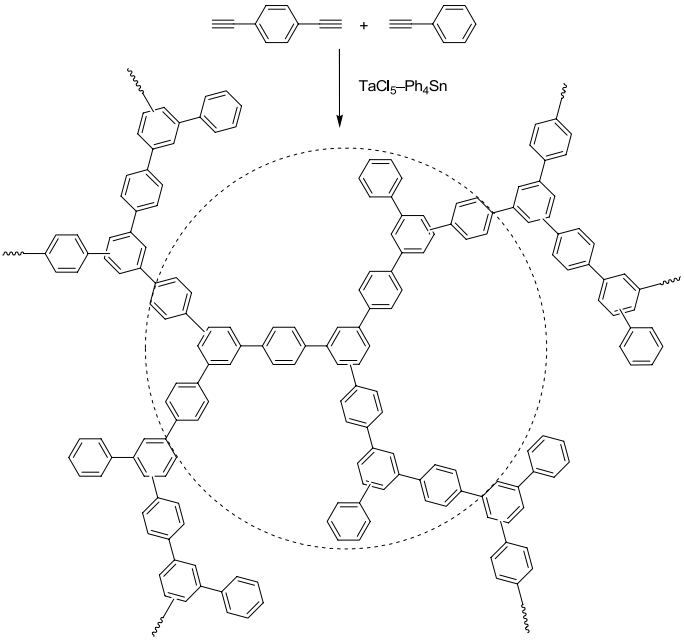

Scheme 26 Synthesis of *hb*-PP through copolycyclotrimerization of aryldiyne with arylmonoyne

Spectral characterization confirmed the proposed hyperbranched architecture of the copolyarylenes. Estimations of the ratio of diyne to monoyne incorporated into the *hb*-PAs revealed that the monoynes functioned as the growth-controlling agents, impeding intracyclotrimerization reactions [86]. As an optimized ratio of diyne to monoyne, 1 : 1.5 has often been found to work well to yield completely soluble, high molecular weight *hb*-PAs. Copolycyclotrimerization of aromatic triynes such as **20** is inherently much more difficult to control. While for aliphatic monoynes like 1-octyne (VI) a monoyne to triyne ratio of 3 : 1 was sufficient to obtain a soluble *hb*-PA, a larger ratio (4 : 1) was necessary for aromatic monoynes such as phenylacetylene (IX) [86, 100].

Detailed structural investigations revealed that even when such a large excess of growth-controlling monoyne was used, the resultant polymers still contained internal cyclic structures. According to the ratio of monoyne to triyne found in *hb*-P(**20**-VI), different propagation modes accounting for the intracyclotrimerization reactions were proposed as depicted in Scheme 27. Taking the 1,2,4- and 1,3,5-isomeric structures of the trisubstituted benzenes into account, the formation of "small"- and "medium"-sized cycles is highly possible. Similar to the silyldiyne homopolycyclotrimerization, the close intramolecular proximity of the two triple bonds originating from an ortho-connection are likely to be terminated by the triple bond of 1-octyne,

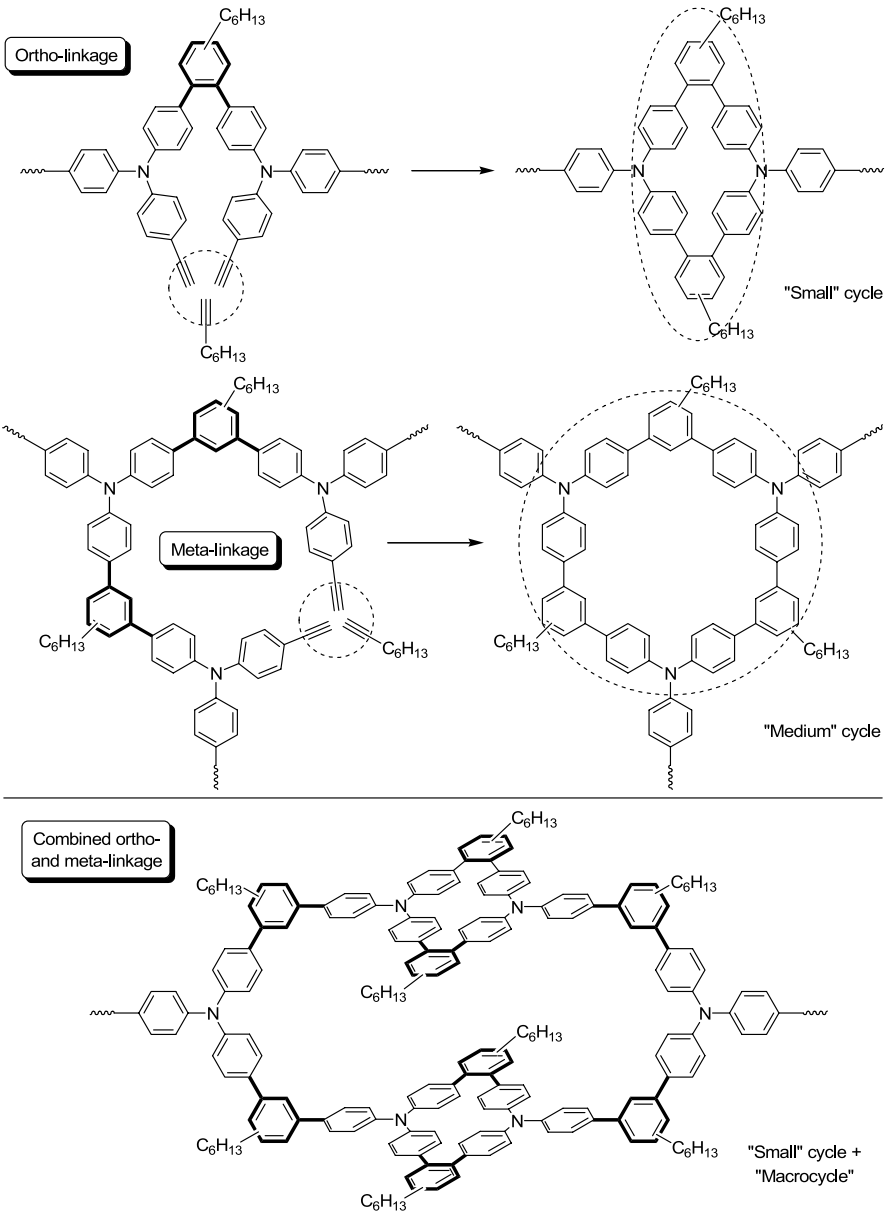

Scheme 27 Formation of intramolecular cyclic structures in alkyne copolycyclotrimerization

thus furnishing a second 1,2,4-trisubstituted benzene ring. This intramolecular "cross-linking" leads to the formation of a small cycle, yet the polymer is still soluble due to the overall pseudo-"linear" propagation mode.

Another possible pathway is the ring closure of the three triyne monomer units connected in a meta fashion with a monoyne via 1,2,4- or 1,3,5-reaction. Such a reaction is likely to produce a medium-sized ring, serving as a core for the macro-dentritic propagation with three growing arms. Para-substituted polymer branches resulting from 1,2,4-cyclotrimerization inherently cannot form any ring structures and may only be involved in the formation of oval-shaped "macrocycles". Such cyclic substructures are possibly formed via combined ortho- and meta-linkages, which exerts little effect on the solubility of the *hb*-PAs, as the overall structure is still propagating in a pseudo-"linear" mode.

2.4.3 Hyperbranched Poly(aroylarylene)s

In the previous section, we have described our successful syntheses of the soluble hyperbranched polymers by the [2 + 2 + 2] (co)polycyclotrimerizations of alkynes initiated by transition metal catalysts. All of the (co)polymers, however, possess regioirregular structures originating from the isomeric structures of 1,3,5- and 1,2,4-trisubstituted benzene rings. This structural irregularity is not necessarily a disadvantage and can actually be beneficial for the solubility and processability of the hyperbranched polymers. On the other hand, it makes it a challenging job to accurately characterize the molecular structures of the polymers by spectroscopic methods. Furthermore, the transition metal catalysts are highly moisture-sensitive and have little tolerance to polar functional groups [93]. The cyclotrimerization of monoynes of benzoylacetylenes catalyzed by the secondary amines is known to proceed in a strictly 1,3,5-regioselective fashion due to the ionic mechanism of the reaction [101–103]. The reaction proceeds in the absence of metallic catalysts: this metal-free feature makes the reaction attractive to us. We therefore explored the possibility of utilizing this cyclotrimerization reaction to prepare *hb*-PAAs from aroyldiynes bearing functional groups. We designed and synthesized a series of new bis(aryl ethynyl ketone)s with various organic and organometallic linkers and investigated their polymerization behaviors (Scheme 28) [104, 105].

It is known that an aroylacetylene undergoes cyclotrimerization in the presence of diethylamine or when refluxed in DMF [101–103]. Supposedly, a small amount of DMF solvent has decomposed at the high temperature (i.e., the boiling point of DMF) to release dimethylamine, which served as the catalytic species [103]. Our attempted polymerization carried out in the presence of diethylamine, however, produced polymers in very low yields (7–21%) [105]. Good to excellent polymer yields were achieved when the bis(aroylacetylene)s were refluxed in DMF/tetralin mixtures for 72 h. Our attempts to shorten the reaction time and to increase the polymer yield by using diphenylamine as the catalyst failed. Use of piperidine as the cata-

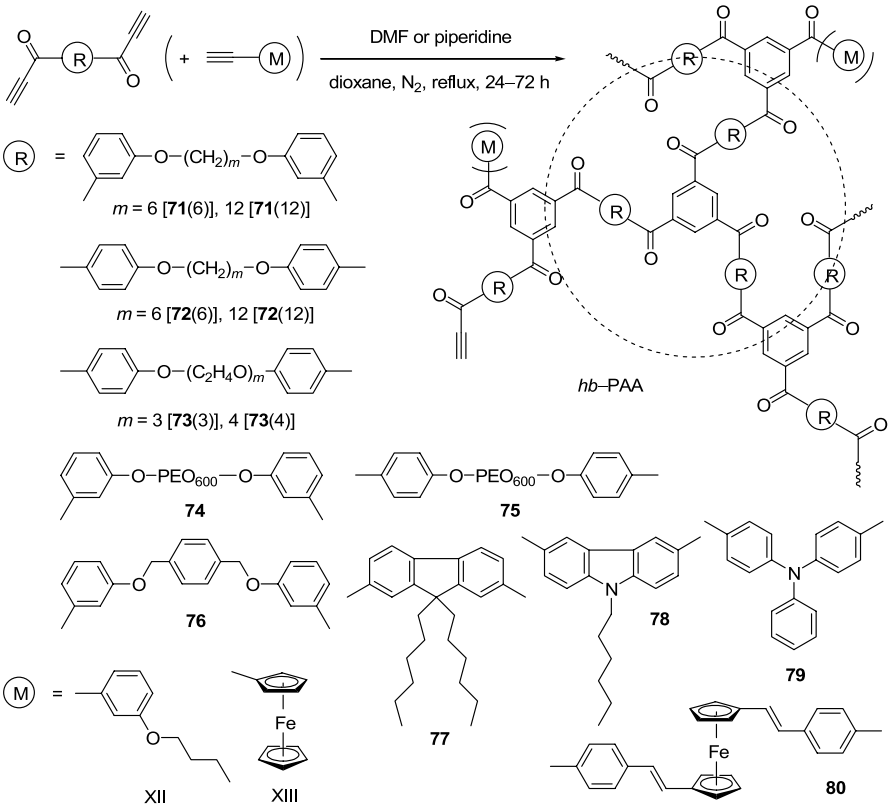

Scheme 28 1,3,5-Regioselective polycyclotrimerization of aroylarylenes

lyst, however, furnished soluble polymers in much shorter reaction times and higher yields: for example, *hb*-P**71**(6) and *hb*-P**73**(4) were obtained in virtually quantitative yields after 24 h reaction.

As proven by the spectroscopic analyses, the aroyldiynes were regioselectively polycyclotrimerized into *hb*-PAAs by piperidine. This regioselectivity stems from the ionic mechanism of the base-catalyzed polycyclotrimerization reaction [106]. Piperidine may have reacted with an aroylethynyl group in a Michael addition mode to form a ketoenamine (*a*), which further reacts with two more aroylethynyl groups to give a dihydrobenzene (*d*; Scheme 29). The piperidine moiety of *d* is removed by its reaction with another aroylethynyl group and aromatization gives a 1,3,5-trisubstituted benzene ring *e*. Repeats of this cycle result in the formation of an *hb*-PAA [105].

Again, with the help of spectral analyses, the hyperbranched structures of the poly(aroylarylene)s were confirmed. Thanks to the 1,3,5-regioselectivity of the cyclotrimerization reaction, the NMR spectra of the *hb*-PAAs were

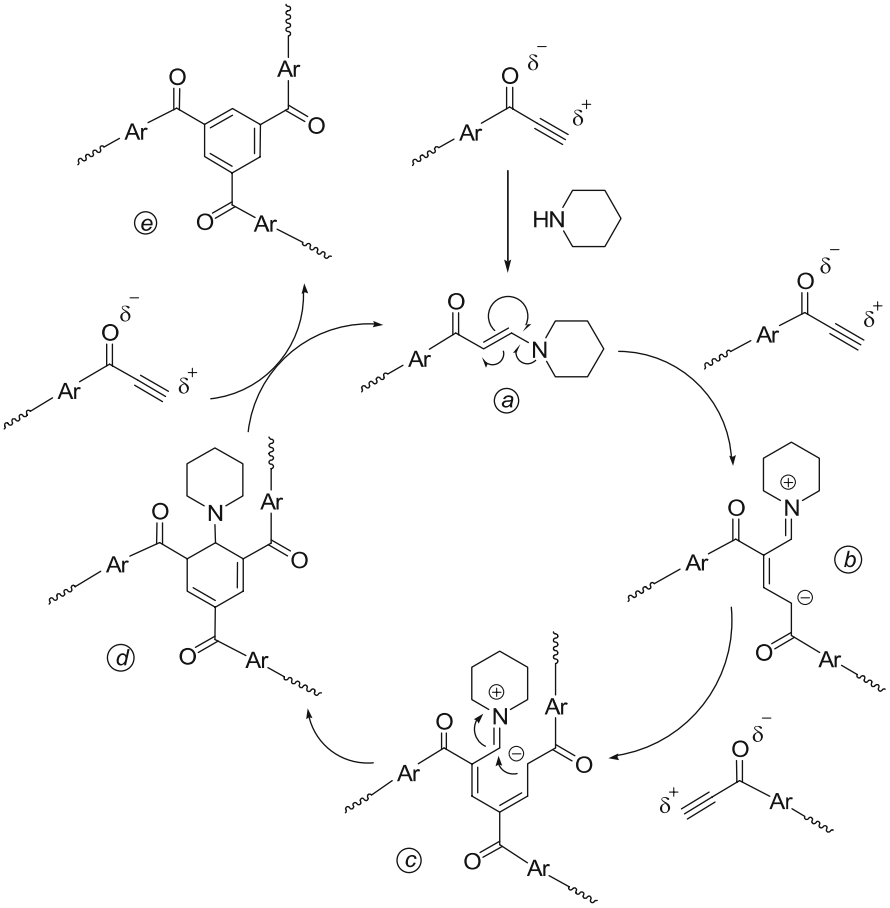

Scheme 29 Proposed mechanism for 1,3,5-regioselective polycyclotrimerization of aryl ethynyl ketone [102, 103]

much simpler, in comparison to their *hb*-PA congeners. The presence of three basic structures of a hyperbranched polymer, viz., *D*, *L* and *T* unites, was readily verified by the number of reacted acetylene triple bonds in the repeat unit (Scheme 30). Because of the structural flexibility of the monomers, especially **71–76**, the polymer branches can also be terminated by an additional dimerization end-capping reaction, in which two alkyne groups of the same diyne molecule react with a ketoenamine to form a new benzene ring. The end group resulting from this back-biting reaction is called "cyclophanic terminal" (T_c). From their corresponding resonance peaks in the ^{1}H NMR spectra, DB values of 78–100% were estimated. These values are much higher than those of the "conventional" hyperbranched polymers, which are commonly in the neighborhood of 50% [107].

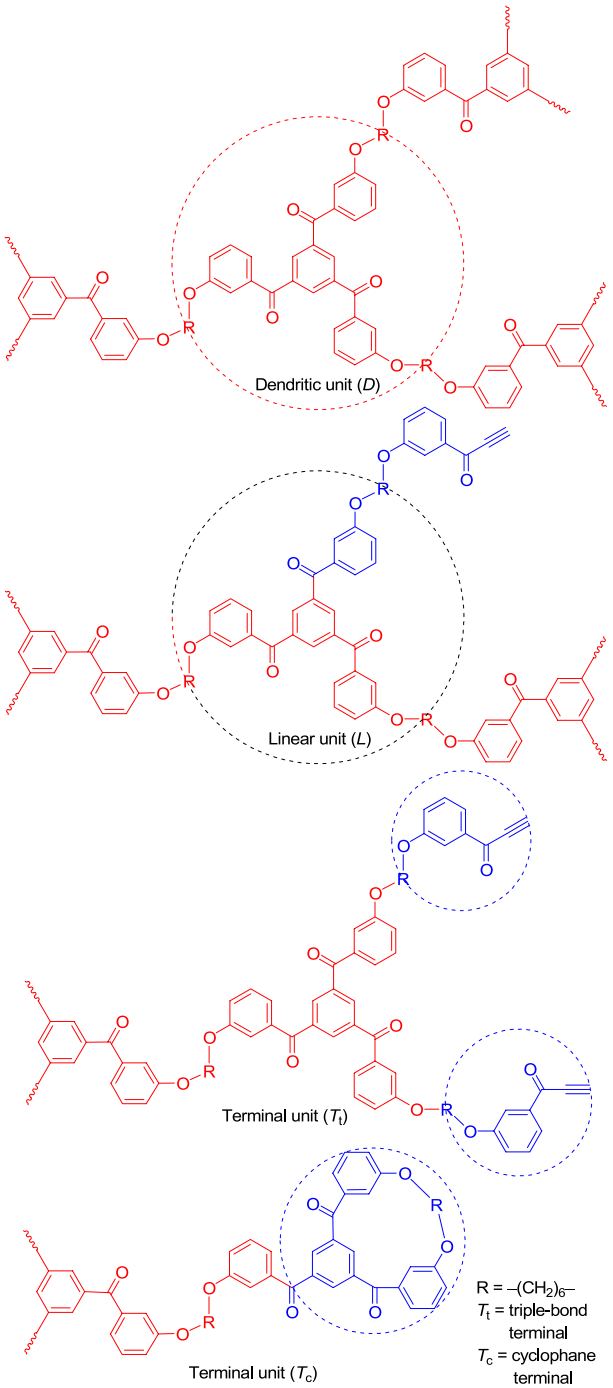

Scheme 30 Molecular structures of *D*, *L* and *T* units of *hb*-PAA

3
Properties

All the herein-described hyperbranched polymers are constructed from triple-bond building blocks and are expected to show unique properties due to their novel π-conjugated structures. Investigation and understanding of the advanced functional properties of the new polymers will aid their development from *macromolecules* of academic curiosity to *materials* of technological value.

3.1
Thermal and Optical Properties

The hyperbranched polymers are carbon-rich macromolecules and show excellent thermal stabilities. The thermal properties of the *hb*-PAs are described below as an example. Their thermal stabilities were evaluated by TGA. Figure 3 shows TGA thermograms of some *hb*-PAs and Table 4 lists their thermal analysis data. The *hb*-PAs were thermally very stable: for instance, *hb*-P**66** lost merely 5% of its weight at a temperature as high as 595 °C. All the polymers, except for *hb*-P(**44**-VI) and *hb*-P(**59**-VI), carbonized in > 50% yields on pyrolysis at 800 °C, with *hb*-P(**45**-V) graphitized in a yield as high as 86% (Table 4, no. 3). The thermal stabilities of the *hb*-PAs are similar to that of linear polyarylenes such as PPP but different from those of linear polyacetylenes such as PH and PPA. The dramatic difference in the thermal stability is mainly due to the structural difference: PPP is composed of thermally stable aromatic rings ($T_d \sim 550$ °C) [108–112], whereas PPA and PH are comprised of labile polyene chains, which start to decompose at temperatures as low as 220 and 150 °C, respectively [113]. The excellent thermal stabilities of the *hb*-PAs

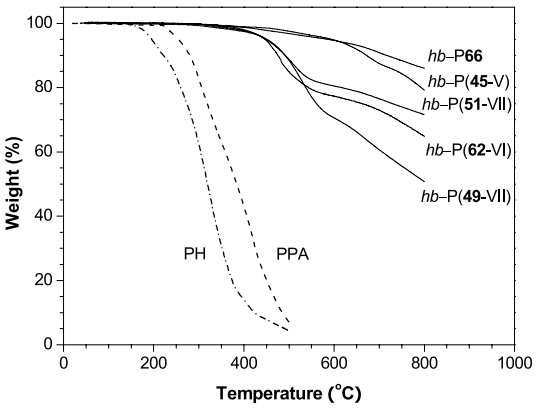

Fig. 3 TGA thermograms of *hb*-PAs; data for linear PH and PPA are shown for comparison

Table 4 Thermal and optical properties of *hb*-PAs

No.	*hb*-PA	T_d [a]	W_r [b]	λ_{em} [c]	Φ_F [d]	T_L [e]	F_{OL} [f]	$F_{t,m}/F_{i,m}$ [g]
1	P(**38**-VI)	452	71 [h]	400	94	59	1016	0.15
2	P(**44**-VI)	440	0	486	14	48	802	0.13
3	P(**45**-V)	585	86	398	49	58	343	0.21
4	P(**45**-VI)	463	66	400	74	69	1265	0.15
5	P(**45**-X)	412	50	397	9	92	900	0.52
6	P(**49**-VII)	449	51	399	46	64	260	0.11
7	P(**50**-V)	467	75	400	31	66	126	0.11
8	P(**50**-VI)	451	70	400	86	48	1000	0.15
9	P(**50**-VII)	459	65	400	98	65	509	0.11
10	P(**52**-VII)	458	53	399	15	44	155	0.08
11	P(**59**-VI)	414	16	402	90	72	2300	0.63
12	P[**60**(5)-V]	487	58	400	7	84	1400	0.36
13	P[**60**(10)-V]	404	83	398	10	83	635	0.36
14	P[**60**(10)-IIX]	474	64	399	20	83	577	0.35
15	P(**61**-VI)	477	70	398	21	49	1034	0.19
16	P(**62**-VI)	463	65	396	28	46	1050	0.17
17	P**66**	595	79	402	1	85	1500	0.43

[a] Temperature (°C) for 5% weight loss
[b] Weight of the residue (%) left at 800 °C unless otherwise specified
[c] Peak of emission spectrum (nm) in DCM solution
[d] Fluorescence quantum yield (%) estimated by using 9,10-diphenylanthracene (Φ_F = 90% in cyclohexane) as standard
[e] Linear transmittance (%)
[f] Optical limiting threshold (mJ/cm^2) defined as the incident fluence at which the nonlinear transmittance is 50% of the initial linear one
[g] Signal suppression (ratio of saturated transmitted fluence to maximum incident fluence)
[h] At 750 °C

thus support the structural analyses by the spectroscopic methods, verifying their hyperbranched polyarylene structures composed of stable aromatic rings instead of labile polyene chains.

Organic molecules containing diyne units readily react upon heating [114–117] and many oligomers or prepolymers with monoyne end groups have been easily converted into thermoset networks [118]. The homo- and copolyynes containing both mono- and diyne moieties are thus expected to undergo facile thermal curing reactions. When *hb*-P(**19**-I) was heated in a DSC cell, it started to release heat at ca. 200 °C due to the commencement of thermally induced cross-linking reactions (Fig. 4). The exothermic reaction peaked at around 270 °C. The second heating scan of the DSC analyses gave almost a flat line parallel to the abscissa in the same temperature region, suggesting that all the acetylene triple bonds have reacted during the first heating scan. The cross-linking reaction of *hb*-P**20** started from ~ 150 °C and peaks at ~ 204 °C. Generally, the homopolyynes commenced to cure at lower tempera-

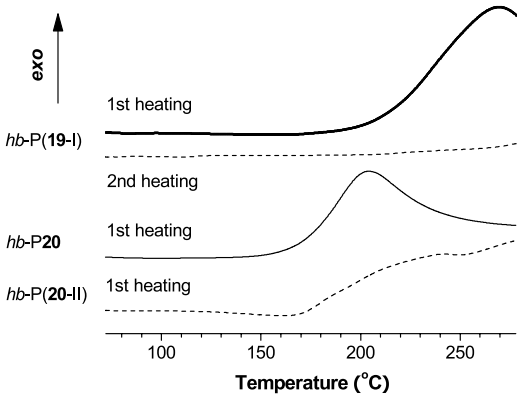

Fig. 4 DSC thermograms of *hb*-PYs measured at a scan rate of 10 °C/min under nitrogen

tures in comparison to their copolyyne congeners, which is probably because the former have more reactive terminal acetylene peripheries [119] and sterically less crowded aryl cores. When the terminal acetylene groups of *hb*-P**20** were end-capped by phenyl groups, the resultant *hb*-P(**20**-II) contained only internal acetylene groups, which needed higher temperatures to initiate and complete its thermal curing reactions. This further manifests the effect of the acetylene reactivity on the thermal curability of the *hb*-PYs.

Many of the hyperbranched polymers contain aromatic chromophores in their π-conjugated structures and should show interesting optical properties [31]. This is indeed the case. For example, *hb*-P**20** carries the TPA chromophore, which is often used as hole-transport materials in the fabrication of light-emitting diodes [120]. The λ_{ab} of triyne **20** appeared at 342 nm (Fig. 5),

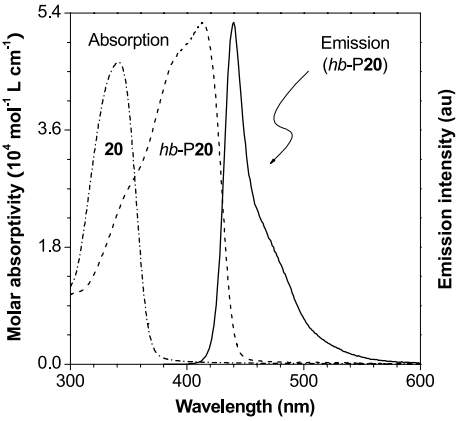

Fig. 5 Absorption spectra of THF solutions of triyne **20** and its polymer *hb*-P**20** (c = 12 μg/mL) and emission spectrum of the *hb*-P**20** solution (λ_{ex} = 368 nm)

which was 43 nm red-shifted from that of TPA [121], thanks to the electronic communication of the peripheral triple bonds with TPA core. The λ_{ab} of *hb*-P**20** was 413 nm, which was further bathochromically shifted from that of **20** by 71 nm, indicative of an extensive π-conjugation in the *hb*-PY. The polymer emitted a blue light of 440 nm upon photoexcitation. The emission was very bright, whose luminance easily goes beyond 1000 cd/m^2 when the polymer was excited by a weak UV lamp with a power of merely 30 mW/cm^2. The absorption and emission spectra of copolymer *hb*-P(**20**-I) resembled those of its homopolymer counterpart *hb*-P**20**, suggesting that the monoyne comonomer has exerted little effect on the electronic transitions of the copolymer.

Other hyperbranched polymers showed similar absorption and luminescence properties. Upon photoexcitation, the *hb*-PA solutions emitted deep-blue to blue-green lights, whose intensities were higher than that of poly(1-phenyl-1-octyne), a well-known highly emissive polyene. The PL efficiencies of the polymers varied with their molecular structures. Polymers *hb*-P(**38**-VI), *hb*-P(**45**-V), *hb*-P(**48**-VI), *hb*-P(**50**-VI), *hb*-P(**50**-VII) and *hb*-P(**59**-VI) exhibited Φ_F values higher than 70%, with *hb*-P(**50**-VII) giving the highest Φ_F value of 98%.

During our search for efficient light-emitting materials, we discovered a group of highly emissive molecules of metalloles such as silole (**57**) and germole (**58**). We synthesized *hb*-PAs containing the metallole moieties and observed a unique phenomenon of cooling-enhanced light emission (Fig. 6) [90]. When a solution of *hb*-P(**57**-VI) was cooled, its PL intensity was dramatically increased. At the low temperatures, the intramolecular rotations of the phenyl rings round the axes of the metallole core were impeded, which efficiently blocked the non-irradiative decay pathways [122]. A similar phenomenon was observed in the system of its congener, *hb*-P(**58**-VI) [89].

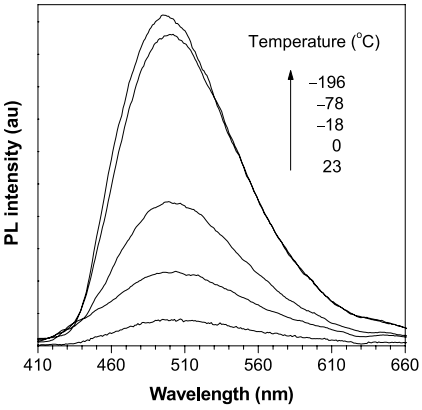

Fig. 6 PL spectra of silole-containing polymer *hb*-P(**57-VI**) in dioxane at different temperatures (c = 10 μM, λ_{ex} = 407 nm)

Figure 7 shows examples of nonlinear attenuation of the optical power of 532 nm laser pulses by *hb*-PA solutions. The transmitted fluence of *hb*-P(**49**-VII) initially increased with an increase in the incident fluence in a linear fashion. It started to deviate from the linearity at an incident fluence of $\sim 260\ mJ/cm^2$ and reached a saturation plateau of $140\ mJ/cm^2$. The optical limiting performance of *hb*-P(**49**-VII) is superior to that of C_{60}, a well-known optical limiter [123]. The three-dimensionally conjugated structure of the *hb*-PAs may have been responsible for their optical nonlinearity, taking into account that C_{60} is a three-dimensionally conjugated buckyball. In comparison to *hb*-P(**49**-VII), *hb*-P(**52**-VII) was a better optical limiter (maximum transmitted fluence $< 100\ mJ/cm^2$) but P(**50**-VI) was a poorer one [93]. Clearly, the optical power-limiting properties of the *hb*-PAs are sensitive to the changes in their molecular structures, which offers opportunities to tune their NLO properties through molecular engineering endeavors.

Second-order NLO-active molecules have attracted much attention due to their attractive photonic applications [124–126]. A major effort in the area has been to efficiently translate large β value into high SHG coefficient d_{33}. The greatest obstacle has been the chromophoric aggregation in the thin films, which often quenches the EO activity in the solid state [127–129]. The chromophoric units of the NLO dyes are usually highly polarized by the push-pull interactions. During film fabrication, the chromophores with large dipole moments tend to compactly pack owing to the strong intermolecular electrostatic interactions, leading to the diminishment or cancellation of the

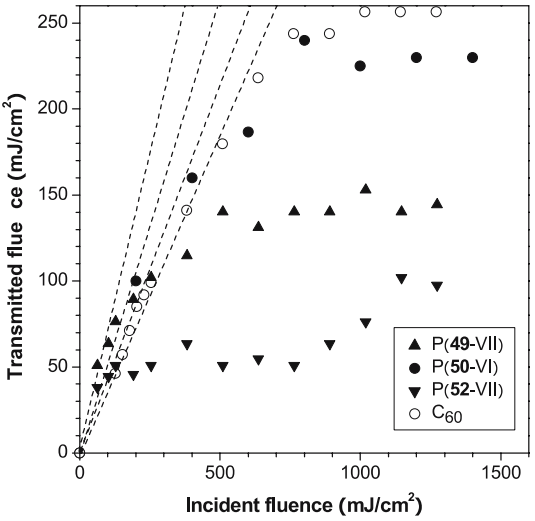

Fig. 7 Optical limiting responses to 8 ns, 532 nm optical pulses, of DCM solutions (0.86 mg/mL) of *hb*-PAs. Data for a toluene solution of C_{60} (0.16 mg/mL) is shown for comparison

NLO effects in the thin films. Hyperbranched polymers should be ideal matrix materials as they offer three-dimensional spatial separation of the NLO chromophores in the spherical architecture, and their void-rich topological structure should help minimize optical loss in the NLO process.

The *hb*-PAEs of *hb*-P**13** and *hb*-P**15** contain NLO-active azo-functionalities, which are soluble, film-forming, and morphologically stable ($T_g > 180\,°C$). Their poled films exhibited high SHG coefficients (d_{33} up to 177 pm/V), thanks to the chromophore-separation and site-isolation effects of the hyperbranched structures of the polymers in the three-dimensional space (Table 5) [28]. The optical nonlinearities of the poled films of the polymers are thermally stable with no drop in d_{33} observable when heated to 152 °C (Fig. 8), due to the facile cross-linking of the multiple acetylenic triple bonds in the *hb*-PAEs at moderate temperatures (e.g., 88 °C).

Advanced photonic devices are often composed of working units with high RI contrasts. The RI values of existing polymers, however, vary in a small range ($n = 1.338–1.710$) [130, 131], which limits the scope of their photonic applications. Theory predicts that molecules consisting of groups with high

Table 5 NLO properties of *hb*-PAEs

hb-PAE	l_f (μm) [a]	d_{33} (pm/V) [b]
hb-P**13**	0.14	177
hb-P**15**	0.42	55

[a] Thickness of solid film
[b] SHG coefficient.

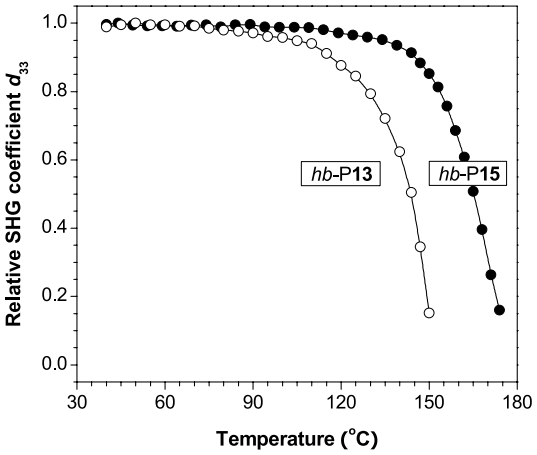

Fig. 8 Decays of SHG coefficients of *hb*-PAEs as a function of temperature

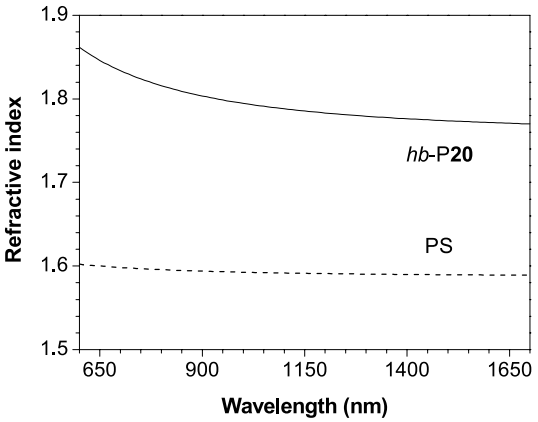

Fig. 9 Wavelength dependence of refractive index of a thin film of *hb*-P**20**. Data for a thin film of PS is shown for comparison

polarizabilities and small volumes can exhibit high refractivities. Polyyne *hb*-P**20** is comprised of electronically mobile aromatic rings and dimensionally slim triple-bond bars and is thus likely to possess high RIs. This proved to the case: a thin film of *hb*-P**20** showed RI values of 1.861–1.770 in the spectral region of 600–1700 nm (Fig. 9), which were much higher than those of well-known "organic glasses" such as PS (n = 1.602–1.589), PMMA (n = 1.497–1.489), and PC (n = 1.593–1.576) [131]. The polyyne film was optically transparent and showed high transmittance in the long wavelength region.

3.2 Patterning and Assembling Behaviors

Thin films of the *hb*-PAPs were highly transparent and absorbed almost no visible light. For example, a film of *hb*-P**32**(5) displayed an optical dispersion as low as 0.009 in the visible region, much superior to those of commercially important organic glasses such as PMMA (0.0175) and polycarbonates (0.0297) [132]. The good film-forming ability and high optical transparency prompted us to utilize the *hb*-PAPs as optical coating materials. The *hb*-PAPs contain many benzyl units, which can readily form radical species, whose recombination will cure or harden the polymers. Indeed, thin films of the hyperbranched polymers were readily cross-linked upon illumination with a UV lamp. Figure 10 shows the formation of insoluble gel upon exposure of a thin film ($\sim$ 1 μm in thickness) of *hb*-P**32**(4) to a UV irradiation. After $\sim$ 20 min exposure, almost the whole film was cross-linked with an F_g of $\sim$ 100%, indicative of a high photosensitivity despite of its irregular hyperbranched structure.

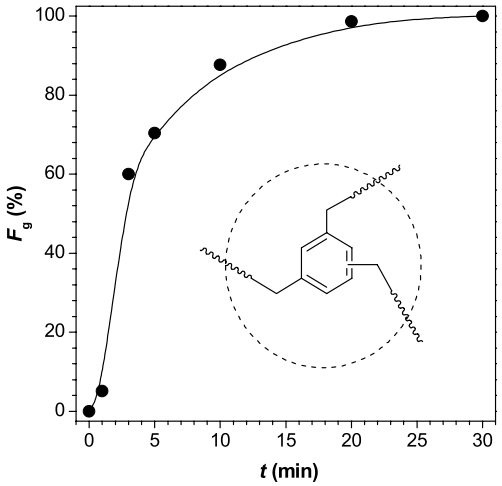

Fig. 10 Plot of gel fraction (F_g) in exposed *hb*-P**32**(4) film versus exposure time (t)

Because of its well-known high photoreactivity, benzophenone has been introduced into natural (e.g., protein) and synthetic polymers (e.g., polyimide) to serve as a photo-cross-linker, and its photoreactions in various polymer matrixes such as PS, PMMA, PC and poly(vinyl alcohol) have been well documented [133–136]. As a matter of fact, benzophenone-containing polyimides such as Ciba-Geigy 412 are commercially available high-performance photoresist materials. The *hb*-PAAs contain numerous aroylbenzene units and, as expected, exhibited very high photo-cross-linking efficiencies. For example, a thin film of *hb*-P**76** on a glass plate could be readily cross-linked by the irradiation with a hand-held UV lamp at room temperature. The cross-linking may have proceeded through the well-established radical mechanism [133–136]: a carbonyl group abstracts a hydrogen atom from a benzyl unit, creating a stable benzyl radical. Coupling or combination of two radicals leads to cross-linking and hence gel formation [105].

Figure 11 depicts the dose effect on the gel formation of *hb*-PAA films (l_F = 1–2 μm) after they have been exposed to a weak UV light with a power of about 1 mW/cm^2. Although the photo-cross-linking conditions had not been optimized, all the four *hb*-PAAs already exhibited much higher sensitivities ($D_{0.5}$ = 43–180 mJ/cm^2) than those of commercial poly(amic ester)-based photoresists ($D_{0.5}$ = 650–700 mJ/cm^2) [137].

Well-resolved patterns with line widths of ∼ 1.0 μm were readily formed when a film of *hb*-P**76** was exposed to a UV dose of 1 J/cm^2 (Fig. 12A). Patterns with submicron resolutions (line width down to 500 nm) were also achievable, as demonstrated by the examples given in panels B and C of Fig. 12. Clearly, *hb*-P**76** is an excellent photoresist material. Similar to *hb*-PAAs, *hb*-PYs were also photosensitive. Well-resolved, defect-free pho-

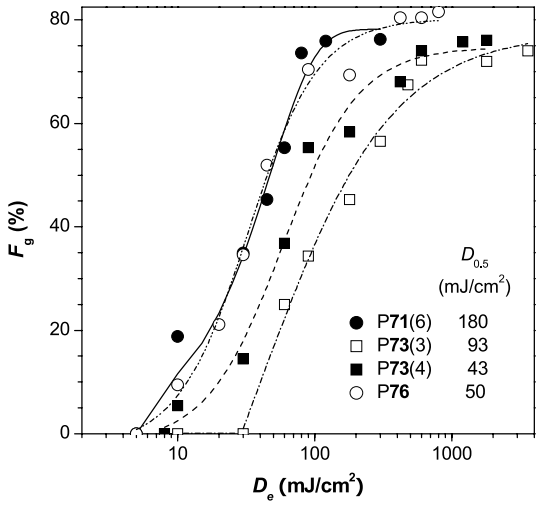

Fig. 11 Plots of gel fractions (F_g) of *hb*-PAA films versus exposure doses (D_e)

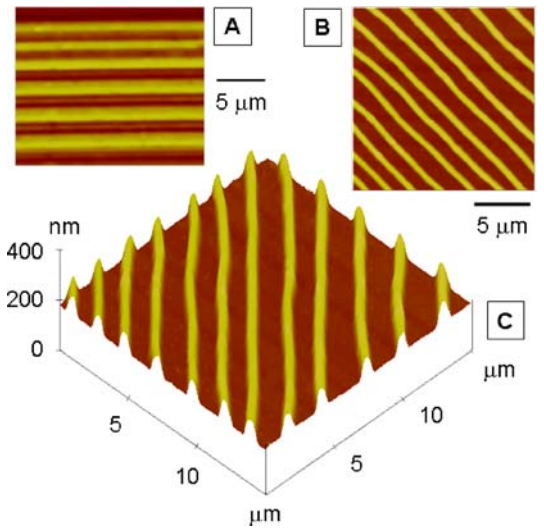

Fig. 12 AFM images of the **A** micro- and **B** and **C** nano-scale patterns obtained from the thin films of *hb*-P**76** exposed to 1 J/cm^2 of UV irradiation

topatterns were readily generated over a large area when a film of *hb*-P**20** was exposed to a UV irradiation (Fig. 13, panels A and C). The magnified photograph clearly revealed sharp edges with excellent shape retention.

Conjugated *hb*-PYs constructed from the building blocks containing TPA units were found to show strong PL in solutions upon excitation [34]. Although the photoinduced cross-linking of the diyne units of *hb*-P**20** will alter

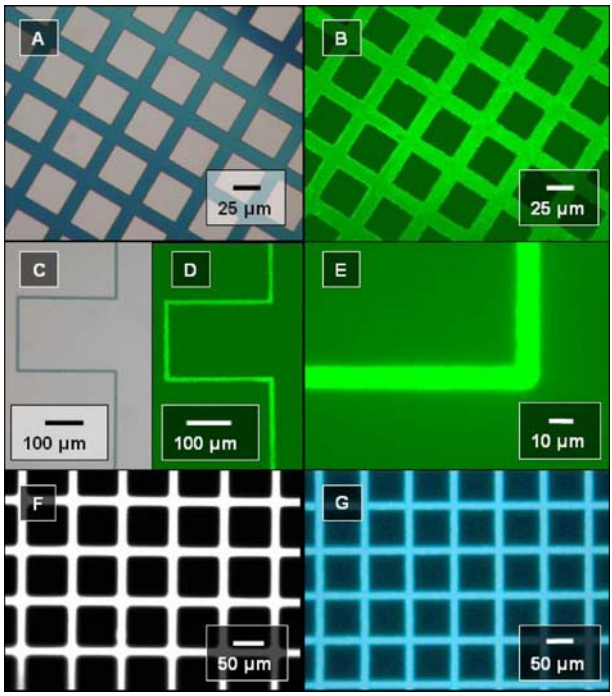

Fig. 13 Negative patterns generated by photolithography of **A**–**E** *hb*-P**20**, **F** *hb-r*-P[**30**(4)-**20**], and **G** *hb*-1,5-P[**30**(4)-**20**]; photographs taken on optical (**A** and **C**) and fluorescence microscopes (**B**, **D**, **E** and **G**)

its conjugation structure, the newly formed cumulene, vinylene and ethynylene may maintain or even enlarge the conjugation extents of the resultant polymer gels. We examined the photogenerated patterns of *hb*-P**20** under a fluorescence microscope. The photographs of different cross-linked patterns of *hb*-P**20** are shown in panels B, D, and E of Fig. 13. All the patterned structures emitted bright light, which is quite remarkable, considering that conjugated polymers often show weak emissions in the solid states or when fabricated into thin films due to the non-radiative energy transfer caused by π-stacking of the polymer chains or defect formation [138]. Since the "conventional" photoresists such as SU-8 are generally nonluminescent and can thus only be used as a passive material [139], the bright emission of our polymers may allow them to be used as an active matrix for the fabrications of liquid crystal displays, light-emitting diodes and other photonic devices [140–142]. It is noteworthy that the negative-tone pattern generated by the regiorandom *hb-r*-PTA containing the TPA core, i.e., *hb-r*-P[**30**(4)–**20**], emitted a white light (Fig. 13F), whereas its regioregular congener, *hb*-1,5-P[**30**(4)–**20**], gives blue fluorescence (Fig. 13G). Clearly, the alteration of the substitution pattern has resulted in a change in the effective conjuga-

tion length, which offers a new way for fine tuning photonic and electro-optical properties of conjugated polymers through a molecular engineering approach.

Template methods have been widely used to fabricate three-dimensional nano- and microstructured patterns. The breath figure process is an elegant yet simple way to generate large arrays of patterned assemblies [143]. When moist air is blown over a polymer solution in an organic solvent, evaporative cooling generates water droplets on the liquid surface. The uniform droplets arrange into a hexagonal array and sink into the polymer solution. Removal of the volatiles (solvent and water) leaves an imprint of the water droplets as a hollow, air-filled, hexagonally ordered, polymeric bubble array. It has been reported that star-shaped polymers and block copolymers form honeycomb morphologies through the evaporation-induced assembly process [144–146]. Other researchers including us have shown that neither star-shaped nor block structure is necessarily needed for the formation of well-defined assembling morphologies [147–151].

We tried to generate assembling structures of *hb*-PYs by employing the breath figure process. Figure 14 shows the photographs of the patterned structures of *hb*-P**20** formed by blowing a stream of moist air over its CS_2 solutions. Hexagonally ordered hollow bubble arrays with void sizes of ca. 10 μm were obtained over a large area. Similar to the patterns generated by UV irradiation through a copper negative mask, the honeycomb patterns obtained from the breath figure process were light-emitting when observed under a fluorescence microscope and can thus potentially be used as an active layer in optical and photonic devices.

As described above, the fabrication of micro- and nano-sized patterns from the hyperbranched polymers as thin layers on defined matrix surfaces has been nicely accomplished. We went one step further and tried to generate free-standing three-dimensional structures. Since *hb*-PAAs can be readily

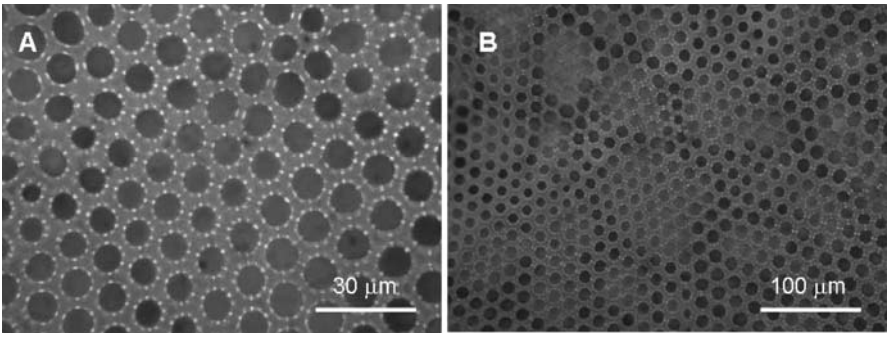

Fig. 14 Optical micrographs of breath figures of *hb*-P**20** obtained from its CS_2 solutions by blow drying in a stream of moist air

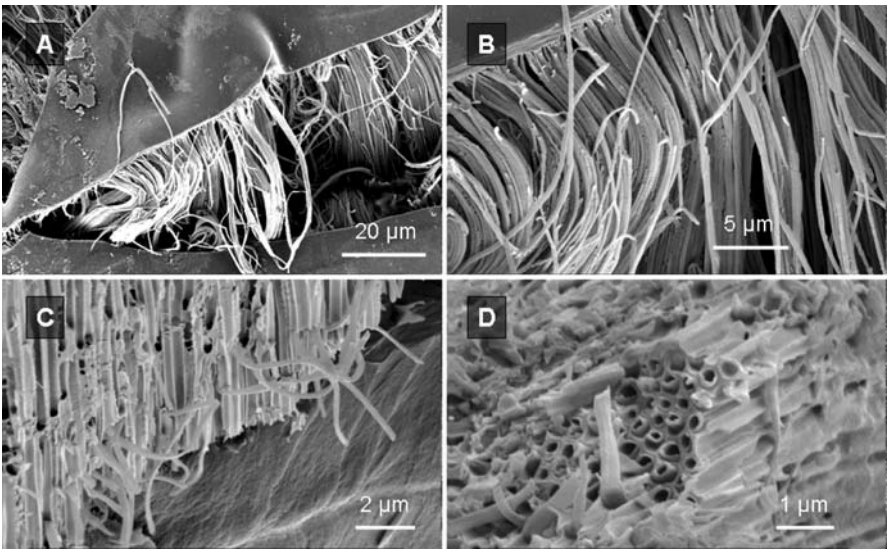

Fig. 15 SEM micrographs of the nanotubes of *hb*-P**71**(6) prepared inside an AAO template with a pore size of ~ 250 nm

prepared from the amine-catalyzed polycyclotrimerizations by simply heating the monomer mixtures, we carried out the polymerization of **71**(6) in the presence of an AAO template. The great advantage of this system is that it does not suffer from any metal residues left behind after the polymerization and the amine catalyst as well as the solvent can be easily removed. Breakage or dissolution of the AAO templates in aqueous sodium hydroxide solution freed the micro structures. SEM micrographs of the templated *hb*-P**71**(6) are shown in Fig. 15. As can be seen from the photos, the *hb*-PAA adopted well the shape of the template pores and formed micrometer-long polymer nanotubes. The hollows of the nanotubes were clearly confirmed by the magnified images given in Fig. 15D.

3.3 Photonic, Magnetic and Catalytic Properties

Acetylenic molecules are versatile ligands in organometallic chemistry [152–154]. Examples of acetylene-metal reactions include facile complexations of one triple bond with $Co_2(CO)_8$ [155–157] and two triple bonds with $CpCo(CO)_2$ (Scheme 31) [158, 159]. The *hb*-PYs contain numerous triple bonds and should be readily metallized through their complexations with the cobalt carbonyls. Upon admixing *hb*-P**20** and the cobalt carbonyls in THF at room temperature, the solution color changed from yellow to brown, accompanied by CO gas evolution. The mixtures remained homogenous towards

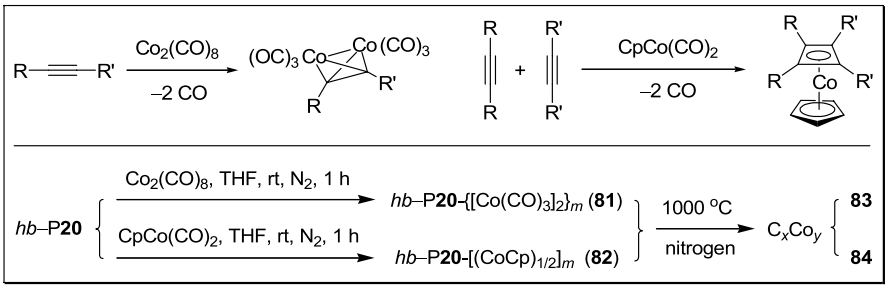

Scheme 31 *Upper panel*: Complex formation between acetylenes and cobalt carbonyls. *Lower panel*: Formation of polymer complexes **81** and **82** via metal complexation and transformation of the complexes into soft ferromagnetic materials **83** and **84** by pyrolytic ceramization

the end of reaction, and the products were purified by pouring the THF solutions into hexane. The polymer complexes are stable in air, whose metal incorporation had been verified by IR analysis [34, 160].

Homogenous yellowish brown-colored films of metallized polymer **81** could be readily prepared by spin coating its freshly prepared complex solution. The films were irradiated through a copper negative mask. Interestingly, the color of the illuminated parts was bleached due to the decomposition of cobalt carbonyl complex, leaving behind the two-dimensional pattern of the photomask (Fig. 16). The enlarged micrograph clearly reveals the sharp edges of the patterns.

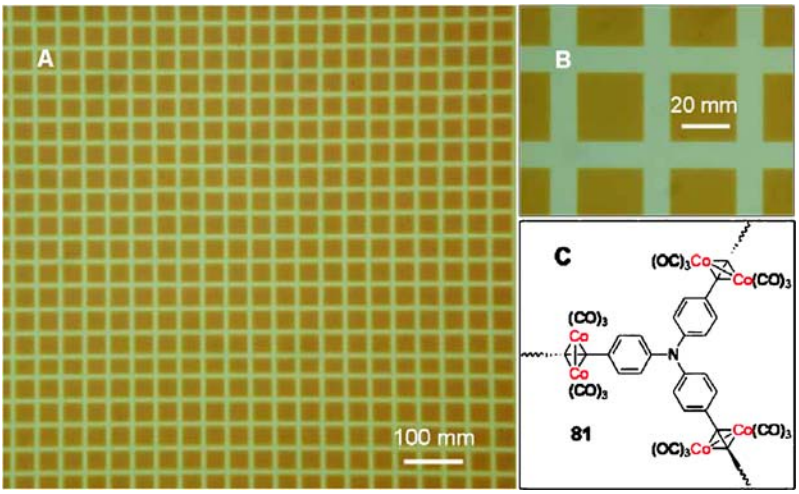

Fig. 16 **A** Optical micrograph of two-dimensional photopattern generated by photolysis of a metallized *hb*-PY (**81**) through a copper-negative mask. **B** Image with a higher magnification and **C** molecular structure of polymer complex **81**

Inspired by the UV light-induced color change of **81**, we studied its optical properties in more details. Figure 17 shows the wavelength-dependent RI values of its unexposed and exposed films. Similar to its parent *hb*-P**20**, the metallized polymer exhibits very high RI values (n = 1.813–1.714) in the spectral region of 600–1600 nm. Remarkably, the RIs drop significantly after the UV irradiation (n = 1.777–1.667). A polymer with such a big RI change is promising for photonic applications: for example, it may serve as photorefractive material in holographic devices [161] or work as high RI optical coating [162].

It has become clear that the carbon-rich *hb*-PYs are readily curable (from ca. 150 °C), thermally stable (up to ca. 550 °C), and pyrolytically carbonizable (yield up to 80% at 900 °C). Furthermore, their triple bonds are easily metallizable by the complexations with cobalt carbonyls. Since the polymer complexes contain a large number of metal atoms, we tried to utilize them as precursors for fabrication of metalloceramics. The pyrolyses of the polyyne-cobalt complexes at 1000 °C for 1 h under nitrogen furnished ceramic products **83** and **84** in 50%–65% yields (cf., Scheme 31). All the ceramics were magnetizable and could be readily attracted to a bar magnet.

The magnetization curves of the magnetoceramics are shown in Fig. 18. With an increase in the strength of the externally applied magnetic field, the magnetization of **83** swiftly increased and eventually leveled off at a saturation magnetization of ~ 118 emu/g, which is much higher than that of the magnet (γ-Fe_2O_3) used in our daily life (M_s = 74 emu/g) [163]. The high M_s value of **83**, along with its powder XRD, XPS and SEM data [160], suggests that the cobalt nanocrystallites in the ceramic are well wrapped by carbonaceous species, which have prevented the cobalt nanoparticles from being oxidized during and after the pyrolysis processes [164]. Evidently, the hyperbranched

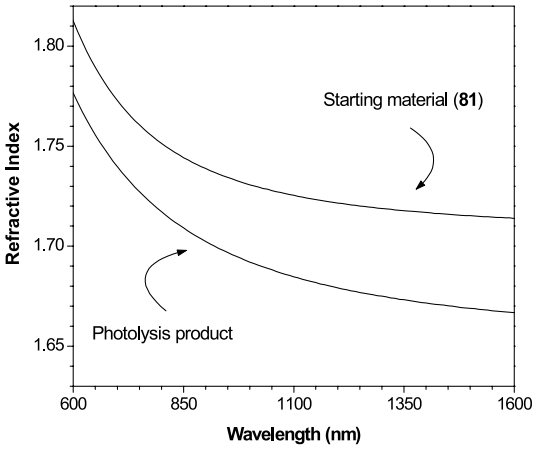

Fig. 17 Refractive indexes of thin films of **81** and its photolysis product

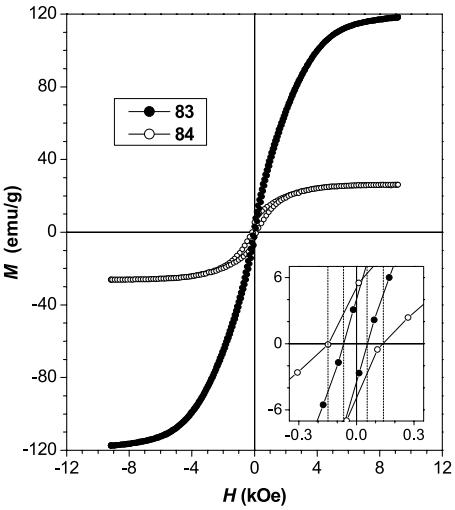

Fig. 18 Plots of magnetization (M) vs. applied magnetic field (H) at 300 K for ceramics **83** and **84**. *Inset*: enlarged portions of the M–H plots in the low strength region of the applied field

polymer complexes are excellent precursors to the magnetic ceramics because their three-dimensional spherical cages have enabled the good retention of the pyrolyzed species and the steady growth of the magnetic crystallites [165]. The M_s value of **84** was somewhat lower ($\sim$ 26 emu/g), which is understandable, because the cobalt content of its precursor complex (**82**) was lower.

Hysteresis loops of the magnetoceramics were very small. From the enlarged H–M plots shown in the inset of Fig. 18, the H_c values of **83** and **84** were found to be 0.058 and 0.142 kOe, respectively. The high magnetizability (M_s up to 118 emu/g) and low coercivity (H_c down to $\sim$ 0.06 kOe) of **83** make it an excellent soft ferromagnetic material, which may have an array of high-technology applications in various electromagnetic systems.

From our previous studies, we knew that hyperbranched polymers containing ferrocene units can be transformed into nano-sized magnetoceramics [165–167]. Taking the advantages of the thermal stability and crosslinking capability of the ferrocene-containing *hb*-PAAs, we first generated organometallic micropatterns by developing a thin film of *hb*-P(**76**-XIII) in dichloroethane, after the film had been exposed to a UV irradiation through a copper negative mask for 30 min. In the second step, these patterns were readily transformed into magnetoceramics by pyrolyzing the microscale grid structures at 1000 °C for 1 h under nitrogen. As can be seen from Fig. 19, the negative-tone photoresist was readily transformed to well-defined, microscopically patterned, iron-containing ceramics with excellent shape retention. Similar to their counterparts prepared in the bulk, the patterned ceramic was also soft ferromagnetic.

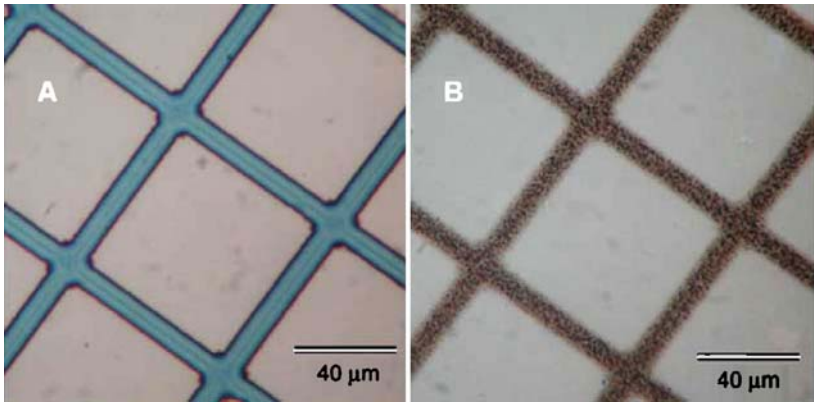

Fig. 19 Photographs of **A** the micropattern fabricated by the photolysis of ferrocene-containing *hb*-P(**76**-XIII) using a copper negative mask and **B** the magnetoceramic pattern generated by the pyrolysis of the micropattern under nitrogen at 1000 °C

Metallic species such as iron, nickel and cobalt are known to catalyze the growth of CNTs in the CVD process [168–170]. Because of the ready thermal curability of the *hb*-PYs, spin-coated films of organometallic polymers **81** and **82** are expected to restrict the agglomeration of the metallic nanoclusters in the CVD process and hence to provide nanoscopic catalyst seeds for the

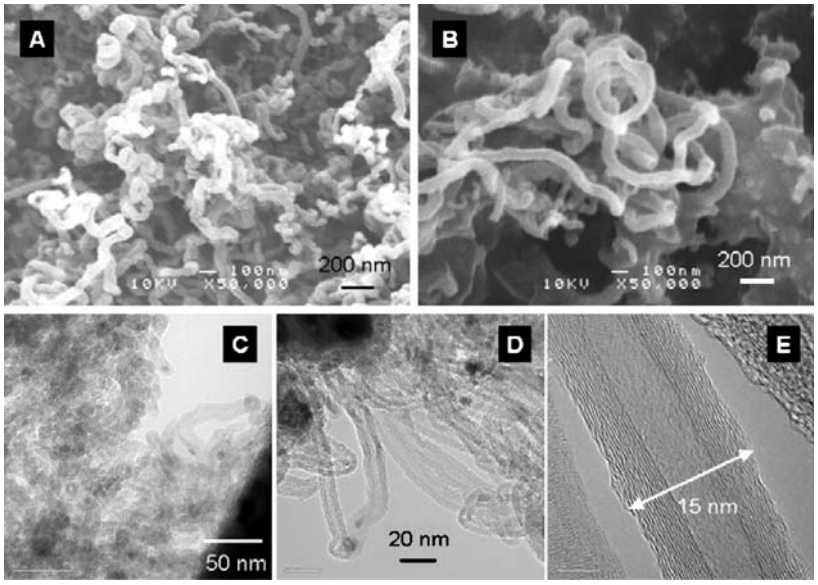

Fig. 20 **A** and **B** SEM and **C–E** TEM micrographs of the CNTs prepared by a CVD process on the silicon wafers spin-coated with **81**

CNT growth. This proved to be the case. Uniform bundles of CNTs were grown by the CVD process at 700 °C with acetylene gas as the carbon source (Fig. 20). The diameters and lengths of the CNTs were alterable by variation of the surface activation as well as the growth time [171]. As expected from a CNT growing temperature below 800 °C [172, 173], the formed CNTs were multiwalled in nature. Their diameters were, however, as small as 15 nm (Fig. 20E).

4 Concluding Remarks

In this review we have briefly summarized the results on the synthesis of a variety of functional hyperbranched polymers from acetylene triple-bond building blocks. Effective polymerization reactions including polycoupling, polyhydrosilylation, polycycloaddition and polycyclotrimerization of mono-, di- and triynes catalyzed by metallic and non-metallic species have been developed, which have enabled the creation of hyperbranched polyynes, polyenes, polyarylenes and polytriazoles with high molecular weights and macroscopic processability in high yields. The new polymerization routes opened and the new structural insights gained offer versatile synthetic tools and valuable guidelines for further developments in this area of research.

Using the triple-bond building blocks in combination with functional groups have resulted in the generation of conjugated polymers with functional properties. The carbon-rich polymers exhibited outstanding thermal stabilities. Incorporation of chromophoric units enabled the modulation of emission colors and efficiencies of the polymers at the molecular level. The numerous aromatic rings in the *hb*-PAs conferred high optical limiting power on the polymers, while the poled films of the azo-functionalized *hb*-PAEs showed stable NLO performance with high SHG coefficients. Combination of the slim diyne linker with the polarizable TPA core results in high optical transparency with exceptionally high photorefractivity. The photosensitive benzyl, benzophenone and diyne units endowed the polymers with photocurability and hence the potential to be used as photoresists and active matrixes in optical devices. The assemblies of hexagonal arrays of breath figures and the micrometer-long polymer nanotubes were obtained from the dynamic and static templating processes. The complexation with the cobalt carbonyls yielded spin-coatable hyperbranched organometallic polymers, whose RIs were readily tuned by UV irradiation. The hyperbranched polymer complexes also served as precursors to advanced soft ferromagnetic ceramics and as catalysts for the growth of CNTs.

Their simple syntheses and ready processability, coupled with their unique structures and useful functionalities, make this group of hyperbranched polymers attractive and promising for an array of high-technology applications.

Acknowledgements This work was partially supported by the Research Grants Council of Hong Kong, the National Science Foundation of China, and the Ministry of Science and Technology of China. We thank all the people involved in this project, some of whose names are given in the references. B.Z.T. thanks the support from the Cao Guangbiao Foundation of the Zhejiang University.

References

1. Flory PJ (1952) J Am Chem Soc 74:2718
2. Wang F, Wilson MS, Rauh RD, Schottland P, Reynolds JR (1999) Macromolecules 33:4272
3. Gao C, Yan D (2001) Macromolecules 34:156
4. Emrick T, Chang HT, Frechet JMJ (1999) Macromolecules 32:6380
5. Jikei M, Chon SH, Kakimoto M, Kawauchi S, Imase T, Watanabe J (1999) Macromolecules 32:2061
6. Russo S, Boulares A, da Rin A, Mariani A, Cosulich ME (1999) Macromol Symp 143:309
7. Ahoni SM (1995) Polym Adv Technol 6:373
8. Frechet JMJ, Henmi M, Gitsov I, Aoshima S, Leduc M, Grubbs RB (1995) Science 269:1080
9. Hawker CJ, Frechet JMJ, Grubbs RB, Dao J (1995) J Am Chem Soc 117:10763
10. Gaynor SG, Edelman SZ, Matyjaszewski K (1996) Macromolecules 29:1079
11. Dworak A, Walach W, Trzebicka B (1995) Macromol Chem Phys 196:1963
12. Suzuki M, Yoshida S, Shiraga K, Saegusa T (1998) Macromolecules 31:1716
13. Magnusson H, Malmström E, Hult A (1999) Macromol Rapid Commun 20:453
14. Bednarek M, Biedron T, Helinski J, Kaluzynski K, Kubisa P, Penczek S (1999) Macromol Rapid Commun 20:369
15. Sunder A, Hanselmann R, Frey H, Mülhaupt R (1999) Macromolecules 32:4240
16. Sunder A, Heinemann J, Frey H (2000) Chem Eur J 6:2499
17. Hult A, Johansson M, Malström E (1999) Adv Polym Sci 143:1
18. Voit B (2003) Comptes Rendus Chimie 6:821
19. Bunz UHF (2001) Acc Chem Res 34:998
20. Negishi EI, Anastasia L (2003) Chem Rev 103:1979
21. Bharathi P, Moore JS (1997) J Am Chem Soc 119:3391
22. Bharathi P, Moore JS (2000) Macromolecules 33:3212
23. Kim C, Chang Y, Kim JS (1996) Macromolecules 29:6353
24. Fomina L, Salcedo R (1996) Polymer 37:1723
25. Hittinger E, Kokil A, Weder C (2004) Angew Chem Int Ed 43:1808
26. Weder C (2005) Chem Commun, p 5378
27. Dong YQ, Li Z, Lam JWY, Dong YP, Feng XD, Tang BZ (2005) Chinese J Polym Sci 23:665
28. Li Z, Qin A, Lam JWY, Dong YQ, Dong YP, Ye C, Williams ID, Tang BZ (2006) Macromolecules 39:1436
29. Jikei M, Chon SH, Kakimoto M, Kawauchi S, Imase T, Watanabe J (1999) Macromolecules 32:2061
30. Lin Q, Long TE (2003) Macromolecules 36:9809
31. Bunz UHF (2000) Chem Rev 100:1605
32. Onitsuka K, Ohshiro N, Fujimoto M, Takei F, Takahashi S (2000) Mol Cryst Liq Cryst 342:159

33. Khan MS, Schwartz DJ, Pasha NA, Kakkar AK, Lin B, Raithby PR, Lewis JZ (1992) Anorg Allg Chem 616:121
34. Häussler M, Zheng R, Lam JWY, Tong H, Dong H, Tang BZ (2004) J Phys Chem B 108:10645
35. Ogawa T (1995) Prog Polym Sci 20:943
36. Hay AS (1998) J Polym Sci Part A: Polym Chem 36:505
37. Hoffmann B, Zanini D, Ripoche I, Burli R, Vasella A (2001) Helv Chim Acta 84:1862
38. Siemsen P, Livingston RC, Diederich F (2000) Angew Chem Int Ed 39:2632
39. Klebansky AL, Grachev IV, Kuznetsova OM (1957) J Gen Chem USSR 27:3008
40. Bohlmann F, Schönowsky H, Inhoffen E, Grau G (1964) Chem Ber 97:794
41. Hawker CJ, Lee R, Frechét JMJ (1991) J Am Chem Soc 113:4583
42. Hölter D, Burgath A, Frey H (1997) Acta Polym 48:30
43. Xiao Y, Wong RA, Son DY (2000) Macromolecules 33:7232
44. Kwak G, Masuda T (2002) Macromol Rap Commun 23:68
45. Kwak G, Takagi A, Fujiki M, Masuda T (2004) Chem Mater 16:781
46. Rao TV, Yamashita H, Uchimaru Y, Sugiyama J, Takeuchi K (2005) Polymer 46:9736
47. Morgenroth F, Müllen K (1997) Tetrahedron 53:15349
48. Huisgen R (1984) In: Padwa A (ed) 1,3-Dipolar Cycloadditions: Introduction, Survey, Mechanism. Wiley, New York
49. Huisgen R, Szeimies G, Moebius L (1967) Chem Ber 100:2494
50. Kolb HC, Finn MG, Sharpless KB (2001) Angew Chem Int Ed 40:2004
51. Rostovtsev VV, Green LG, Fokin VV, Sharpless KB (2002) Angew Chem Int Ed 41:2596
52. Scheel A, Komber H, Voit B (2004) Macromol Rapid Commun 25:1175
53. Voit B (2005) J Polym Sci Part A: Polym Chem 43:2679
54. Qin A, Haeussler M, Lam JWY, Tse KKC, Tang BZ (2006) Polym Prepr 47(2):681
55. Chan TR, Hilgraf R, Sharpless KB, Fokin VV (2004) Org Lett 6:2853
56. Himo F, Lovell T, Hilgraf R, Rostovtsev VV, Noodleman L, Sharpless KB, Fokin VV (2005) J Am Chem Soc 127:210
57. Zhang L, Chen X, Xue P, Sun HHY, Williams ID, Sharpless KB, Fokin VV, Jia G (2005) J Am Chem Soc 127:15998
58. Majireck MM, Weinreb SM (2006) J Org Chem 71:8680
59. Sergeyev VA, Shitikov VK, Chernomordik YA, Korshak VV (1975) Appl Polym Symp 26:237
60. Sergeyev VA, Shitikov VK, Kurapov AS, Antonova-Antipova IP (1989) Polym Sci USSR 31:1300
61. Srinrivasan R, Farona MF (1988) Polym Bull 20:359
62. Chalk AJ, Gilbert AR (1972) J Polym Sci: Part A-1 10:2033
63. Bracke W (1972) J Polym Sci: Part A-1 10:2097
64. Xu K, Tang BZ (1999) Chinese J Polym Sci 17:397
65. Xu K, Peng H, Sun Q, Dong Y, Salhi F, Luo J, Chen J, Hunag Y, Zhang D, Xu Z, Tang BZ (2000) Macromolecules 35:5821
66. Zheng R, Dong H, Peng H, Lam JWY, Tang BZ (2004) Macromolecules 37:5196
67. Xu K, Peng H, Huang Y, Xu Z, Tang BZ (2000) Polym Prepr 41(2):1245
68. Li Z, Lam JWY, Dong YQ, Dong YP, Sung HHY, Williams ID, Tang BZ (2006) Macromolecules 39:6458
69. Saito S, Yamamoto Y (2000) Chem Rev 100:2901
70. Lautens M, Klute W, Tam W (1996) Chem Rev 96:49
71. Melikyan GG, Nicholas KM (1995) In: Stang PJ, Diederich F (eds) Modern Acetylene Chemistry. Wiley, Weinheim, p 99

72. Schore NE (1991) In: Trost BM, Flemming I (eds) Comprehensive Organic Synthesis. Pergamon, Oxford 5:1129
73. Vollhardt KPC (1984) Angew Chem Int Ed 23:539
74. Mori N, Ikeda S, Odashima K (2001) Chem Commun p 181
75. Tekeuchi R, Tanaka S, Nakaya Y (2001) Tetrahedron Lett 42:2991
76. Yamamoto Y, Ogawa R, Itoh K (2000) Chem Commun, p 549
77. Ozerov OV, Ladipo FT, Patrick BO (1999) J Am Chem Soc 121:7941
78. Johnson ES, Balaich GJ, Rothwell IP (1997) J Am Chem Soc 119:7685
79. Masuda T, Mouri T, Higashimura T (1980) Bull Chem Soc Jpn 53:1152
80. Cotton FA, Hall WT (1980) Inorg Chem 19:2352
81. Bruck MA, Copenhaver AS, Wigley DE (1987) J Am Chem Soc 109:6525
82. Cotton FA, Hall WT (1981) Inorg Chem 20:1285
83. Strickler JR, Wexler PA, Wigley DE (1988) Organometallics 7:2067
84. Cotton FA, Wilkinson G (1988) Advanced Inorganic Chemistry, 5th ed, Chap 19B. Wiley, New York
85. Jhingan AK, Maier WF (1987) J Org Chem 52:1161
86. Zheng R, Häussler M, Dong H, Lam JWY, Tang BZ (2006) Macromolecules 39:7973
87. Häußler M, Lam JWY, Peng H, Zheng R, Tang BZ (2003) Polym Prepr 44(1):1177
88. Häußler M, Lam JWY, Zheng R, Peng H, Luo J, Chen J, Law CCW, Tang BZ (2003) Comptes Rendus Chimie 6:833
89. Law CCW, Chen J, Lam JWY, Peng H, Tang BZ (2004) J Inorg Organomet Polym 14:39
90. Chen J, Peng H, Law CCW, Dong YP, Lam JWY, Williams ID, Tang BZ (2003) Macromolecules 36:4319
91. Zheng R, Dong H, Tang BZ (2005) In: Abd-El-Azi A, Carraher C, Pittman C, Sheats J, Zeldin M (eds) Macromolecules Containing Metal- and Metal-like Elements. Wiley, New York
92. Peng H, Luo J, Cheng L, Lam JWY, Xu K, Dong Y, Zhang D, Huang Y, Xu Z, Tang BZ (2002) Opt Mater 21:315
93. Peng H, Cheng L, Luo J, Xu K, Sun Q, Dong Y, Salhi F, Lee PPS, Chen J, Tang BZ (2002) Macromolecules 35:5349
94. Peng H, Lam JWY, Tang BZ (2005) Polymer 46:5746
95. Peng H, Lam JWY, Tang BZ (2005) Macromol Rapid Commun 26:673
96. Peng H, Zheng R, Dong H, Jia D, Tang BZ (2005) Chin J Polym Sci 23:1
97. Häußler M, Dong H, Lam JWY, Zheng R, Qin A, Tang BZ (2005) Chin J Polym Sci 23:567
98. Dong H, Lam JWY, Häußler M, Zheng R, Peng H, Law CCW, Tang BZ (2004) Curr Trends Polym Sci 9:15
99. Kong X, Lam JWY, Tang BZ (1999) Macromolecules 32:1722
100. Zheng R, Lam JWY, Peng H, Häußler M, Law CCW, Tang BZ (2003) Polym Prepr 44(2):770
101. Balasubramanian K, Selvaraj S, Venkataramani PS (1980) Synthesis p 29
102. Pigge FC, Ghasedi F, Rath NJ (2002) J Org Chem 67:4547
103. Matsuda K, Nakamura N, Iwamura H (1994) Chem Lett, p 1765
104. Dong H, Zheng R, Lam JWY, Häußler M, Tang BZ (2004) Polym Prepr 45(2):825
105. Dong H, Zheng R, Lam JWY, Häußler M, Tang BZ (2005) Macromolecules 38:6382
106. Saito S, Yamamoto Y (2000) Chem Rev 100:2901
107. Jikei M, Kakimoto M (2001) Prog Polym Sci 26:1233
108. Schluter AD, Wegner G (1993) Acta Polym 44:59
109. Tour JM (1994) Adv Mater 6:190
110. Johnen NA, Kim HK, Ober CK (1994) ACS Symp Ser 579:298

111. Kumar U, Neenan TX (1995) ACS Symp Ser 614:4084
112. Watson MD, Fechtenkotter A, Mullen K (2001) Chem Rev 101:1267
113. Masuda T, Tang BZ, Higashimura T, Yamaoka H (1985) Macromolecules 18:2369
114. Badarau C, Wang ZY (2004) Macromolecules 37:147
115. Armistead JP, Houser EJ, Keller TM (2000) Appl Organomet Chem 14:253
116. Gandon S, Mison P, Sillion B (1996) ACS Symp Ser 624:306
117. Rutherford DR, Stille JK, Elliott CM, Reichert VR (1992) Macromolecules 25:2294
118. Hergenrother PM (1990) In: Kroschwitz JI (ed) Concise Encyclopedia of Polymer Science & Engineering. Wiley, New York, p 5
119. Beckham HW, Keller TM (2002) J Mater Chem 12:3363
120. Mochizuki H Hasui T, Kawamoto M, Ikeda T, Adachi C, Taniguchi Y, Shirota Y (2003) Macromolecules 36:3457
121. Berlman IB (1971) Handbook of Fluorescence Spectra of Aromatic Molecules, 2nd ed. Academic Press, New York
122. Chen J, Xie Z, Lam JWY, Law CCW, Tang BZ (2003) Macromolecules 36:1108
123. Tang BZ, Leung SM, Peng H, Yu NT, Su KC (1997) Macromolecules 30:2848
124. Lee M, Katz HE, Erben C, Gill DM, Gopalan P, Heber JD, McGee DJ (2002) Science 298:1401
125. Shi Y, Zhang C, Zhang H, Bechtel JH, Dalton LR, Robinson BH, Steier WH (2000) Science 288:119
126. Burland DM, Miller RD, Walsh CA (1994) Chem Rev 94:31
127. Marder SR, Cheng LT, Tiemann BG, Friedli AC, Blanchard-Desce M, Perry JW, Skindhøj J (1994) Science 263:511
128. Dalton LR, Harper AW, Ren A, Wang F, Todorova G, Chen J, Zhang C, Lee M (1999) Ind Eng Chem Res 38:8
129. Luo J, Ma H, Haller M, Barto RR (2002) Chem Commun, p 888
130. Seferis JC (1989) Refractive Indices of Polymers. In: Brandrup J, Immergut EH (eds) Polymer Handbook, 3rd ed. Wiley, New York, p VI/451
131. Mills NJ (1990) In: Kroschwitz JI (ed) Concise Encyclopedia of Polymer Science & Engineering. Wiley, New York, p 683
132. Xu K, Peng H, Tang BZ (2001) Polym Prepr 42(1):555
133. Luo Y, Leszyk J, Qian YD, Gergely J, Tao T (1999) Biochemistry 38:6678
134. Hasegawa M, Horie K (2001) Prog Polym Sci 26:259
135. Turro NJ (1978) Modern Molecular Photochemistry. In: Benjamin-Cummings Publ. Co. (ed) Modern Molecular Photochemistry. Menlo Park, California
136. Qu BJ, Xu YH, Shi FW (1992) Macromolecules 25:5215
137. Kim K-H, Jang S, Harris FW (2001) Macromolecules 34:8925
138. Hua JL, Lam JWY, Dong H, Wu L, Wong KS, Tang BZ (2006) Polymer 47:18
139. Wang Y, Bachman M, Sims CE, Li GP, Allbritton NL (2006) Langmuir 22:2719
140. Kim C, Burrows PE, Forrest SR (2000) Science 288:831
141. Sirringhaus H, Kawase T, Friend RH, Shimoda T, Inbasekaran M, Wu W, Woo EP (2000) Science 290:2123
142. Garnier F, Hajlaoui R, Yassar A, Srivastava P (1994) Science 265:1684
143. Bunz UHF (2006) Adv Mater 18:973
144. Widawski G, Rawiso M, Francois B (1994) Nature 369:387
145. Jenekhe SA, Chen XL (1999) Science 283:372
146. de Boer B, Stalmach U, Nijland H, Hadziioannou G (2000) Adv Mater 12:1581
147. Srinivasarao M, Collings D, Philips A, Patel S (2001) Science 292:79
148. Peng J, Han Y, Li B (2004) Polymer 45:447
149. Tang BZ (2001) Polym News 26:262

150. Lam JWY, Tang BZ (2005) Acc Chem Res 38:745
151. Salhi F, Cheuk KKL, Sun Q, Lam JWY, Cha JAK, Li G, Li B, Luo J, Chen J, Tang BZ (2001) J Nanosci Nanotechnol 1:137
152. Babudri F, Farinola GM, Naso F (2004) J Mater Chem 14:11
153. Long NJ, Williams CK (2003) Angew Chem Int Ed 42:2586
154. Bunz UHF (2003) J Organomet Chem 683:269
155. Newkome GR, He EF, Moorefield CN (1999) Chem Rev 99:1689
156. Chauhan BPS, Corriu RJP, Lanneau GF, Priou C, Auner N, Handwerker H, Herdtweck E (1995) Organometallics 14:1657
157. Chan WY, Berenbaum A, Clendenning SB, Lough AJ, Manners I (2003) Organometallics 22:3796
158. Nishihara H, Kurashina M, Murata M (2003) Macromol Symp 196:27
159. Altmann M, Bunz UHF (1995) Angew Chem Int Ed 34:569
160. Häußler M, Lam JWY, Zheng R, Dong H, Tong H, Tang BZ (2005) J Inorg Organomet Polym Mat 15:519
161. Hendrickx E, Engels C, Schaerlaekens M, Van Steenwinckel D, Samyn C, Persoons A (2002) J Phys Chem B 106:4588
162. Lu C, Guan C, Liu Y, Cheng Y, Yang B (2005) Chem Mater 17:2448
163. Tang BZ, Geng Y, Lam JWY, Li B, Jing X, Wang X, Wang F, Pakhomov AB, Zhang XX (1999) Chem Mater 11:1581
164. O'Handley RC (2000) Modern Magnetic Materials: Principles and Applications. Wiley, New York, p 491
165. Sun Q, Xu K, Peng H, Zheng R, Häußler M, Tang BZ (2003) Macromolecules 36:2309
166. Sun Q, Lam JWY, Xu K, Xu H, Cha JAK, Zhang X, Jing X, Wang F, Tang BZ (2000) Chem Mater 12:2617
167. Häußler M, Sun Q, Xu K, Lam JWY, Dong H Tang BZ (2005) J Inorg Organomet Polym 15:67
168. Chatterjee AK, Sharon M, Baneriee R, Neumann-Spallart M (2003) Electrochim Acta 48:3439
169. Huang ZP, Wang DZ, Wen JG, Sennett M, Gibson H, Ren ZF (2002) Appl Phys A 74:387
170. Deck CP, Vecchio K (2006) Carbon 44:267
171. Häußler M, Tse KC, Lam JWY, Tong H, Qin A, Tang BZ (2006) Polym Mat Sci Eng 95:213
172. Lu JQ, Kopley TE, Moll N, Roitman D, Chamberlin D, Fu Q, Liu J, Russell TP, Rider DA, Manners I, Winnik MA (2005) Chem Mater 17:2227
173. Lu JQ, Rider DA, Onyegam E, Wang H, Winnik MA, Manners I, Cheng Q, Fu Q, Liu J (2006) Langmuir 22:5174

Editor: Kwang-Sup Lee